ACS PHYSICAL CHEMISTRY Au
AN OPEN ACCESS JOURNAL OF THE AMERICAN CHEMICAL SOCIETY

pubs.acs.org/physchemau
Perspective

Mastering Femtosecond Stimulated Raman Spectroscopy: A Practical Guide

Pauline G. Lynch, Aritra Das, Shahzad Alam, Christopher C. Rich, and Renee R. Frontiera*

Cite This: ACS Phys. Chem Au 2024, 4, 1−18
Read Online

ABSTRACT: Femtosecond stimulated Raman spectroscopy (FSRS) is a powerful nonlinear spectroscopic technique that probes changes in molecular and material structure with high temporal and spectral resolution. With proper spectral interpretation, this is equivalent to mapping out reactive pathways on highly anharmonic excited-state potential energy surfaces with femtosecond to picosecond time resolution. FSRS has been used to examine structural dynamics in a wide range of samples, including photoactive proteins, photovoltaic materials, plasmonic nanostructures, polymers, and a range of others, with experiments performed in multiple groups around the world. As the FSRS technique grows in popularity and is increasingly implemented in user facilities, there is a need for a widespread understanding of the methodology and best practices. In this review, we present a practical guide to FSRS, including discussions of instrumentation, as well as data acquisition and analysis. First, we describe common methods of generating the three pulses required for FSRS: the probe, Raman pump, and actinic pump, including a discussion of the parameters to consider when selecting a beam generation method. We then outline approaches for effective and efficient FSRS data acquisition. We discuss common data analysis techniques for FSRS, as well as more advanced analyses aimed at extracting small signals on a large background. We conclude with a discussion of some of the new directions for FSRS research, including spectromicroscopy. Overall, this review provides researchers with a practical handbook for FSRS as a technique with the aim of encouraging many scientists and engineers to use it in their research.

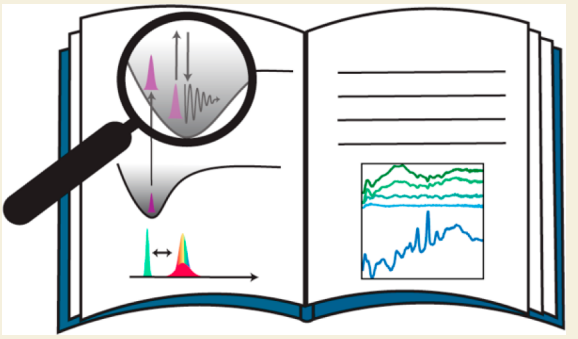

KEYWORDS: *femtosecond stimulated Raman spectroscopy, FSRS, stimulated Raman spectroscopy, ultrafast spectroscopy, vibrational spectroscopy, Raman scattering*

1. INTRODUCTION

It has been over two decades since the first introduction of femtosecond stimulated Raman spectroscopy (FSRS) to the scientific community,[1−4] and as of June 2023, there are now over 3300 papers that include the term "femtosecond stimulated Raman."[5] The popularity of FSRS comes from its ability to track structural evolution with Raman spectroscopy on the ultrafast time scale. FSRS monitors the response of vibrational modes to photoexcitation, which allows researchers to monitor changes in molecular and material structure on excited electronic states and map out the multidimensional nuclear coordinates associated with various photophysical and photochemical processes, like internal conversion,[6,7] intersystem crossing,[8−12] singlet fission,[13−17] electron transfer,[18−23] proton transfer,[24−28] and photoisomerization.[8,29−34] FSRS opens the door to unraveling the molecular motions that dictate relaxation pathways of photoexcited systems and helps to identify the required structural modifications for targeted photodriven functionalities of different systems. FSRS is complementary to other structurally sensitive ultrafast techniques, such as transient infrared spectroscopy, impulsive stimulated Raman spectroscopy (ISRS), and ultrafast X-ray spectroscopies. However, FSRS is compatible with nearly any type of sample and is implemented with tabletop ultrafast lasers with moderate pulse durations, which makes it one of the more accessible techniques in this field.

FSRS is a three-pulse technique and is formally a six-wave mixing spectroscopy, although it makes use of molecular resonances to facilitate signal generation. In the FSRS, we use a femtosecond actinic pump pulse to excite the system to a more energetic electronic state. After a time delay (τ) from the photoexcitation, a picosecond Raman pump and a femtosecond probe pulse act on the system to create vibrational

Received: July 12, 2023
Revised: October 2, 2023
Accepted: October 2, 2023
Published: October 21, 2023

https://doi.org/10.1021/acsphyschemau.3c00031
ACS Phys. Chem Au 2024, 4, 1−18

coherences and generate the stimulated Raman signals (SRS) that hold the time-resolved structural information about the system. As the time delay between the Raman pump−probe pair and actinic pump is easily tunable, it allows us to record multiple stimulated Raman spectra as the system structurally evolves with time following photoexcitation. This approach maps out changes in nuclear coordinates on reactive potential energy surfaces, thereby enabling "molecular movies" of a reacting system.

In its early days, it was claimed that FSRS could break the Heisenberg uncertainty principle and attain information with simultaneously high spectral and temporal resolution. While careful analysis of a complete fitted FSRS data set can, indeed, provide information on time scales faster than would be allowed by the spectral bandwidth, it is of course subject to the same laws of physics as any other experiment. In FSRS, it is possible to extract information on very fast time scales by considering the evolution of vibrational coherences throughout the entire time-resolved experiment—essentially by performing a global fit of the entire data set rather than analyzing a single spectrum at a single time point. Two such examples of the power of this approach are the rapid frequency changes in hydrogen out-of-plane modes in photoexcited rhodopsin[29] and the oscillatory frequency evolution in photoexcited green fluorescent protein.[26] In both instances, information on time scales faster than vibrational dephasing times is extracted by careful analysis of the complete FSRS data set and by considering the evolution of the vibrational coherences during spectral generation. This issue of time resolution in FSRS is somewhat analogous to statements about imaging techniques, such as PALM (photoactivated localization microscopy) and STORM (stochastic optical reconstruction microscopy), which break the optical diffraction limit—these techniques do, indeed, obtain information at length scales well below the diffraction limit, but this requires data processing and some prior knowledge of the system of interest. The same holds true for FSRS.

Apart from its excellent temporal and spectral resolution, the FSRS technique has several other benefits. It is compatible with most solvents, including water, and is easily combined with a standard optical microscope for spectromicroscopy measurements.[35] Given that it is self-heterodyned with the broadband probe pulse, it is possible to acquire a complete vibrational spectrum in a single shot provided the user has high-quality filters to access the low-frequency spectral region. Additionally, the FSRS can be tuned to make use of resonance enhancement in ground or excited electronic states, thereby providing large signal enhancements and species selectivity. These attributes, along with extensive theoretical background, are covered in great detail in a series of previous review articles.[36−40]

While this technique can address fundamental questions regarding ultrafast molecular dynamics, the realization of FSRS experimentally requires some degree of technical expertise. In this article, we will address some of the practical factors faced by researchers performing FSRS, including considerations in selecting beam generation methods, aligning the three beams to set up for a FSRS experiment, choosing a sample, and analyzing data. Our goal is to outline a practical guide for researchers who are planning to adopt FSRS in their own research.

2. EXPERIMENTAL SECTION

2.1. Laser Requirements

FSRS experiments require three synchronized laser beams—an actinic pump, a Raman pump, and a Raman probe. These beams are usually provided by a single ultrafast laser, most commonly a chirped pulse amplified Ti:sapphire system with fundamental pulse durations in the range of 20−200 fs; although increasingly, FSRS is implemented with fiber-based laser systems.

Unlike ISRS, FSRS does not require ultrashort (<10 fs) pulses, and thus, the fundamental pulse duration and subsequent pulse compression is not particularly crucial for the experiment provided the pulses are short and intense enough to achieve the nonlinear optical processes described below. The repetition rate of the fundamental laser impacts the choice of detection system, described later, as well as the overall duty cycle. The total power output needed is dictated by the number of nonlinear processes needed to generate the desired pulses at their desired wavelengths. For example, a FSRS system with a tunable-wavelength Raman pump pulse will likely require more output power than a system with a Raman pump wavelength fixed at the fundamental frequency.

FSRS experiments require three laser pulses with specific characteristics, which are called the actinic pump pulse, the Raman pump pulse, and the probe pulse. Figure 1 shows the different options for each of the three beams, and the benefits and drawbacks of each are discussed in the following section.

2.2. Beam Generation

2.2.1. Probe. Given that the stimulated Raman signals are self-heterodyned with the probe, the stability and spectral bandwidth of the probe are critical to performing a high-quality FSRS experiment. First, the probe pulse must be stable, both on the time scale of the detection system and on the time scale of the total experiment. For a kHz repetition rate system with single-shot detection, we aim for root-mean-square (RMS) deviations in the probe intensity of less than 0.5%. This means that the small Raman pump-induced changes occurring on top of the broad probe background will be readily visible, although this is dependent on the particular sample of interest, including its Raman cross section and overall concentration. Second, the probe pulse spectrum must be smoothly varying with no highly sloped regions, as these lead to large baseline issues in Raman gain spectra. Finally, the probe pulse should have a spectrally broad range to capture the entire desired spectral window, typically ranging from 250 to 2000 cm^{-1}. The broad spectrum results in a temporally narrow probe pulse; therefore, the Raman interaction can be initiated with precise timing in the excited-state potential energy surface.

To achieve these requirements, the most common method of generating a probe pulse is to generate a white light continuum in a medium with a modest nonlinear refractive index and a high damage threshold. These media include sapphire,[6,13,14,20,35,41−55] CaF_2,[8,9,56−62] $GdVO_4$,[63] yttrium aluminium garnet (YAG),[64−67] liquids such as water,[24,68−70] noble gases,[71] or photonic crystal fibers.[72−74] The choice of material will determine the spectral range of the probe and so must be considered carefully for the given application. For continuum generation in the visible and near-infrared regions of the spectrum, sapphire is a common choice because of its high damage threshold. For applications in the ultraviolet, CaF_2 is commonly used, although generally with a rotation or translation stage to minimize photodamage issues.[40] Photonic

https://doi.org/10.1021/acsphyschemau.3c00031
ACS Phys. Chem Au 2024, 4, 1−18

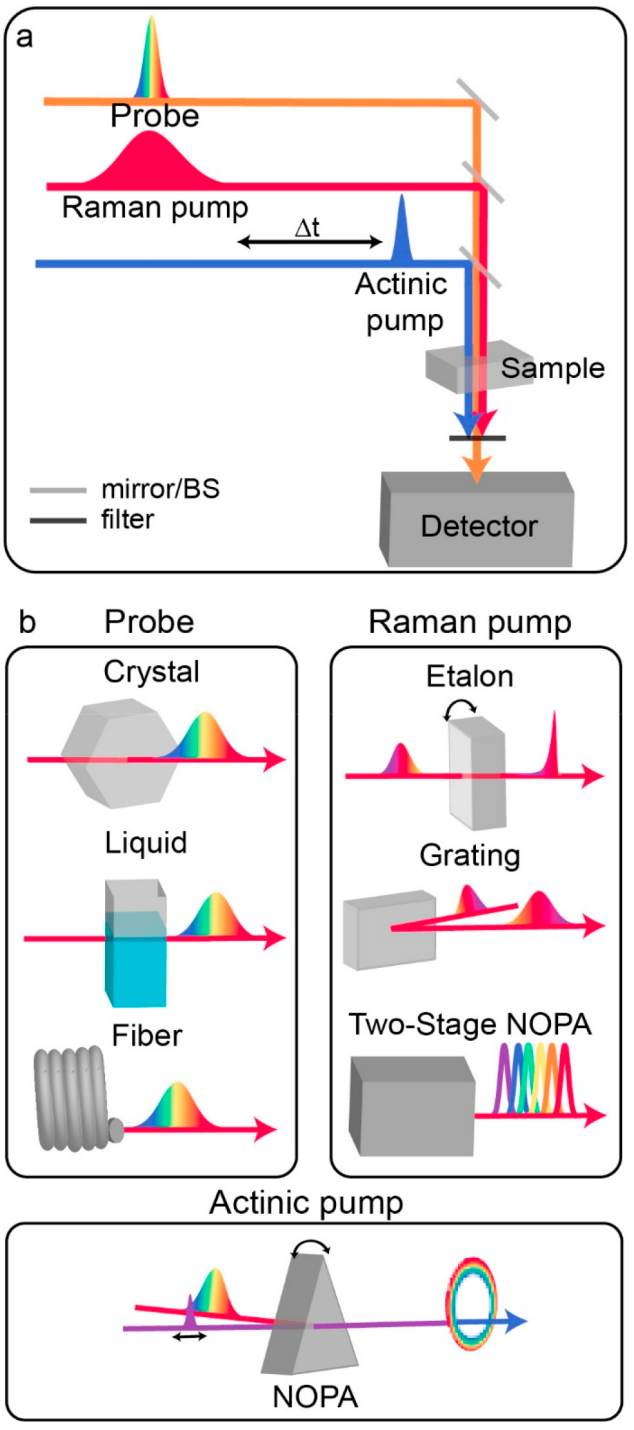

Figure 1. (a) Basic FSRS schematic. BS = beamsplitter. (b) Examples of common methods of generating the three beams necessary for FSRS. The femtosecond probe can be generated in crystals, liquid flow cells, or photonic crystal fibers. The picosecond Raman pump pulse must be picoseconds in duration and is commonly generated with approaches such as an etalon, grating filter, or two-stage noncollinear optical parametric amplifier (NOPA). The actinic pump is commonly generated using femtosecond NOPA (fs-NOPA).

crystal fibers or gas-filled fibers have been used in low-pulse energy systems, although these have lower stability.[40] In some situations, the power provided by continuum generation is insufficient, in which case other methods, such as femtosecond noncollinear optical parametric amplification (fs-NOPA)[31,75−77] and broadband up-converted multicolor array (BUMA) can be used for probe generation.[45,78−80] Ernsting et al. have used fs-NOPA to generate a high-power tunable probe for FSRS; however, the spectral range is only limited to a 1200 cm^{-1} window.[81]

Most of these pulse generation approaches generate broadband pulses with a high degree of chirp. While it is not necessary to compress the pulses for FSRS, it is common to do so in order to obtain broadband Raman gain spectra in a single acquisition. If the probe pulse is highly chirped to the extent that individual spectral components will not be temporally overlapped with the Raman pump pulse maximum, then the resulting stimulated Raman signal will contain only a small portion of the spectrum in which the relative signal intensities will be distorted by the wavelength-dependent temporal overlap between the two pulses. For example, if the probe is chirped to the extent that portions of the spectrum do not overlap temporally with the Raman pump, then there will be no stimulated Raman signal in the spectral region of the probe. While a small amount of chirp relative to the picosecond duration Raman pump pulse will likely not cause significant distortion, a large amount of chirp can result in poor temporal overlap between the fs probe and ps Raman pump pulse and lead to a greater extent of distorted spectral intensities. Common pulse compression methods involve the use of prism compressors,[16,39,82] acousto-optic filters,[83] grating filters,[84,85] or chirped mirrors.[86] Correction for third-order dispersion in the probe spectrum is generally not necessary for most FSRS experiments.

2.2.2. Raman Pump. To generate a stimulated Raman spectrum with high spectral resolution, it is essential to use a spectrally narrow and temporally long Raman pump. Overall, the spectral resolution in a ground-state FSRS spectrum is limited by the bandwidth of the Raman pump and the instrument response function. If the Raman pump temporal duration is shorter than the vibrational dephasing time of the mode(s) of interest, it will truncate those vibrational coherences and broaden the measured Raman line widths. Thus, typical Raman pump pulse durations used in FSRS are on the order of picoseconds, which are longer than most ground-state vibrational dephasing times and nearly all vibrational dephasing times on electronic excited states, particularly for solution-based samples. Additionally, the wavelength of the Raman pump pulse is crucial to the success of the experiment. Wavelengths that are considerably off-resonant with excited-state electronic transitions for a given sample often exhibit low Raman cross sections. However, wavelengths that are directly on resonance can lead to the generation of additional four-wave mixing processes [such as transient absorption (TA) or stimulated emission], which may interfere with the SRS generation.[53] Wavelengths that are preresonant generally work quite well, although electronic resonances can shift rapidly for highly reactive excited-state surfaces. Therefore, there are numerous methods that have been adopted to generate a Raman pump pulse for FSRS. Fundamentally, these approaches all involve generating a picosecond pulse from a femtosecond pulse, which is usually an inherently lossy process.

The most straightforward method to generate a Raman pump pulse is to opt for a fixed wavelength and spectrally narrow the broadband fundamental output of the laser.[40] Common approaches used involve the integration of optical etalons or grating filters. The etalon acts as a Fabry−Perot

https://doi.org/10.1021/acsphyschemau.3c00031
ACS Phys. Chem Au 2024, 4, 1−18

resonator by transmitting only a specific range of wavelengths and converting a portion of the broadband femtosecond fundamental into a narrowband picosecond Raman pump pulse by selectively removing unwanted frequencies. The output wavelength from an etalon can be tuned across the range of a few nanometers by changing the tilt angle, although the tuning range is small compared with other options for achieving a truly tunable Raman pump (Figure 2a).

The use of an etalon produces a time-asymmetric pulse that works exceptionally well to produce very spectrally narrow line shapes, compared with other filtering techniques, and has been shown to reduce the nonresonant background in similar techniques, such as sum-frequency generation spectroscopy.[87,88] It is important to select an etalon that has a large free-spectral range relative to the fundamental laser bandwidth such that there are no sidebands that also lead to stimulated Raman signal generation, as seen in Figure 2a,b at −2° and −3°. The etalon is extremely easy to integrate into a FSRS system but can be expensive and may be susceptible to damage.

Another option for spectrally narrowing the fundamental laser beam is to use a grating filter (Table 1). This can be a less expensive and more tunable option compared with an etalon but requires additional expertise to build and align.[87] A grating filter acts as a spectral filter by diffracting and transmitting only a specific range of wavelengths while blocking most of the spectral component. The grating filter approach results in Raman pump pulses that have easily tunable temporal widths and allows for a small degree of frequency tuning. Using a second-order diffraction double pass grating filter, Kang et al. recently reported the lowest spectral resolution in a FSRS experiment (2.5 cm^{-1}).[52] Grating filters can also easily be adapted for frequency comb FSRS, which can aid in the discrimination of Raman peaks from narrow transient absorption features.[83] The primary drawback of using a fixed wavelength Raman pump pulse, regardless of spectral filtering method, is the inability to tune the wavelength of the pump pulse across a large range to access different electronic resonances.

There are many options for generating a narrowband, tunable Raman pump, and these approaches have seen several advancements for use in FSRS over recent years. The key factors to consider when selecting a method are the spectral window in which the pulse can be tuned, the resultant bandwidth of the stimulated Raman signal, and the conversion efficiency of the tunable pulse. Some methods for generating a tunable Raman pump are listed in Table 2, along with their spectral resolution, conversion efficiency, and tunability ranges.

While implementing a tunable Raman pump can often be more complicated than a fixed wavelength, it allows access to a wider range of samples, which benefit from the resonantly enhanced signal. It also enables researchers to strategically choose multiple Raman pump wavelengths to study different regions on the excited-state potential energy surface and build up a more comprehensive picture of excited-state dynamics.[48] However, if the Raman pump is resonant with an electronic transition, it can deplete the excited-state population and drive additional transitions, which compete with FSRS signals,[95] including Raman pump-induced transient absorption (TA) signals, which can create large backgrounds that distort or cover up FSRS signals.[96] This can be avoided by choosing a wavelength that is preresonant with the molecular system's electronic states,[96] thereby gaining some resonance enhancement in the stimulated Raman signal but minimizing the TA signals. Researchers have also developed a novel method of modulating Raman pump wavelength to reduce the TA features.[55] Previous work demonstrates that exciting on or near electronic resonance results in dispersive line shapes,

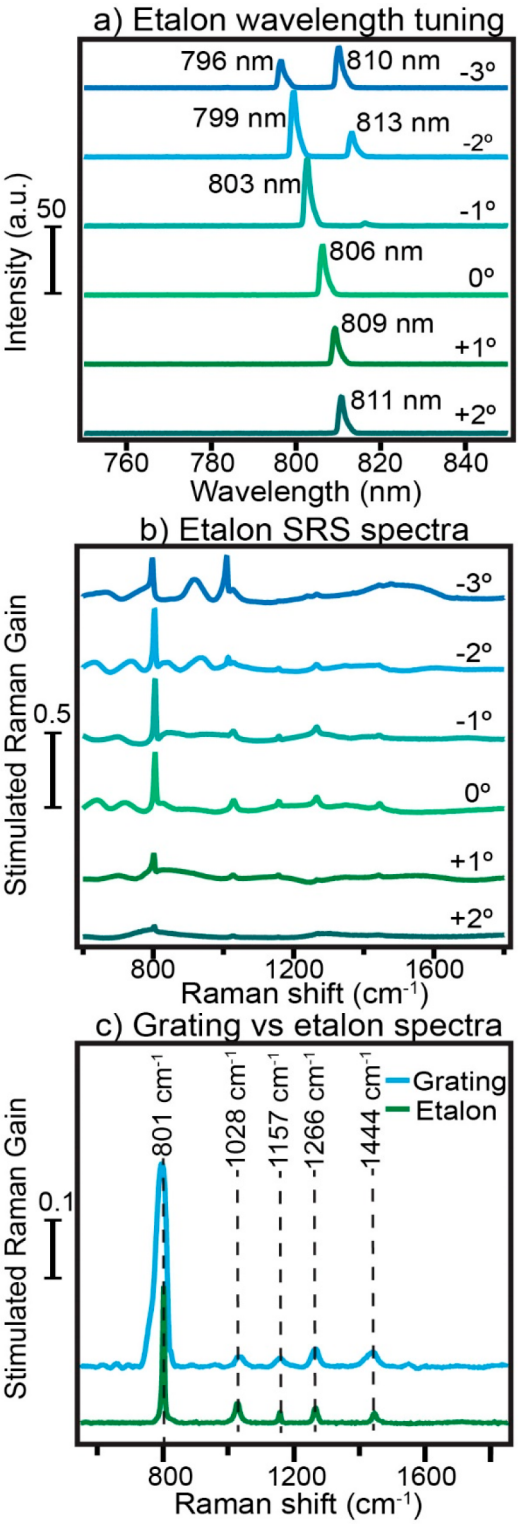

Figure 2. (a) Tuning the Raman pump wavelength with the etalon angle. (b) Stimulated Raman spectra of cyclohexane as a function of etalon angle. (c) Stimulated Raman spectra of cyclohexane using a grating filter (blue) and an etalon (green) with corresponding peak amplitudes and widths in Table 1 below. Grating λ = 798 nm, and etalon λ = 806 nm.

https://doi.org/10.1021/acsphyschemau.3c00031
ACS Phys. Chem Au 2024, 4, 1−18

Table 1. Stimulated Raman Gain with Etalon or Grating[a]

mode frequency (cm^{-1})	etalon Raman gain amplitude ($\times 10^2$)	etalon Raman gain width (cm^{-1})	grating Raman gain amplitude ($\times 10^2$)	grating Raman gain width (cm^{-1})
801	20.01 ± 0.39	7.4 ± 0.2	30.03 ± 0.72	31.6 ± 0.9
1028	2.62 ± 0.04	15.3 ± 0.3	1.73 ± 0.06	27.9 ± 1.3
1157	1.61 ± 0.06	6.6 ± 0.3	1.09 ± 0.04	25.5 ± 1.0
1266	2.29 ± 0.04	14.6 ± 0.4	2.91 ± 0.02	26.6 ± 0.3
1444	1.20 ± 0.07	11.6 ± 0.8	2.08 ± 0.05	39.8 ± 1.1

[a]Stimulated Raman gain in a 2 mm cyclohexane cuvette using an etalon or a grating filter to spectrally narrow the Raman pump. Amplitudes and widths were obtained by fitting the peaks in Figure 2c to a Gaussian function. Spectra were acquired for 3 s each. For both the etalon and grating filter, the Raman pump pulse energy was 0.8 μJ, the pulse duration was approximately 2 ps, and the beam diameter was 15 μm, which led to a peak flux of 500 GW/cm^2. The probe pulse energy was 0.025 μJ, the pulse duration was approximately 100 fs, and the beam diameter was 3 μm, which gave a peak flux of 7000 GW/cm^2.

which complicates the resulting FSRS spectra (Figure 3). Liu et al. have demonstrated that tuning the Raman pump wavelength can reduce these TA effects while maintaining high signal-to-noise ratio (SNR).[48,53,96]

Once the Raman pump is generated, it usually passes through a manual delay stage and a chopper. The delay stage is used to adjust the time delay between the Raman pump and the probe during alignment, and the chopper modulates the Raman pump and is important for the detection scheme, which we discuss in Section 2.4.

2.2.3. Actinic Pump. The final beam to consider is the actinic pump, which will photoexcite the sample. Therefore, the wavelength must overlap with the sample's electronic absorption band. Most researchers opt for tunable NOPAs to generate their actinic pump pulses since tunability is desirable to expand the range of molecules that can be probed. After the tunable beam is generated, compression of the actinic pump pulse is often required to ensure short pulses that allow for ultrafast instrumental time resolution. There are several options for compressing the pulse, including prism compressor,[21,97] chirped mirrors,[98,99] and deformable mirrors.[100] After this, the actinic pump is sent into a motorized delay stage to control the time delay between the actinic pump and the temporally overlapped Raman pump and probe pair.

The effective time resolution of a FSRS experiment is determined primarily by two factors: the cross-correlation of the actinic pump and Raman probe pulse and the vibrational dephasing time of the vibrational modes under investigation.[40] Therefore, a temporally narrower actinic pulse can be helpful for observing dynamics at short time delays. The temporal information obtained during acquisition of a single spectrum represents a combination of vibrational dephasing time and cross correlation of the actinic pump and probe pulses, which we discuss in more detail in Section 2.6.

2.3. Spatial and Temporal Overlap

In this section, we outline the general procedure for the optimal alignment of the three beams. We will discuss the alignment procedure and share what we have learned on how to improve this process and troubleshoot. In general, we align the Raman probe first since all signal is collected on top of the probe, and so, it is critical that it is well aligned through the sample and detector. Then, the Raman pump pulse is overlapped with the probe pulse by maximizing the stimulated Raman signal. Finally, the actinic pump pulse is overlapped with the probe pulse through a cross-correlation measurement. In this approach, it is important that the probe beam has the smallest relative beam waist at the sample position so that the Raman pump and actinic pump can have slightly larger beam waists and still interact in the same region.

The Raman pump spatial and temporal overlap with the probe is optimized by maximizing the stimulated Raman signal of a standard. Cyclohexane is a common standard to use, but the standard should be selected on the basis of its similarities to the sample of interest—they should be of the same phase and have similar thickness and have Raman peaks in the same spectral region. For solid samples, a thin sheet of polystyrene or diamond works well. The stimulated Raman signal is obtained by adjusting both the temporal and spatial overlap of the Raman pump with the probe. The extent of the temporal overlap can also determine the extent of background signals, such as cross-phase modulation (XPM). XPM will result in an unstable, oscillating baseline and can obscure the stimulated Raman gain. To avoid this, we use vibrating motors taped on the Raman pump delay stage. The vibrators randomize the phase relationship between the Raman pump and probe such that the averaged Raman spectrum contains fewer contributions from XPM. It is important to quantify the known maximum stimulated Raman signal for each laser system to ensure the ideal spatial and temporal overlap between the Raman pump and probe. For example, fluctuations in the magnitude of the standard's stimulated Raman signal can indicate that the beam-focusing conditions are changing. A benchmark for the stimulated Raman signal in a system can ensure proper alignment for each experiment. Once the

Table 2. Tunable Raman Pump Generation Methods[a]

method	Raman pump bandwidth (cm^{-1})	Raman spectral bandwidth (cm^{-1})	conversion efficiency (%)	tuning range (nm)
second harmonic spectral compression (SHSC) with spectral filtering[89]	10		0.075−0.25	330−750
narrowband optical parametric amplifier (NB-OPA)[90]	36	38	0.03−0.68	470−670
second harmonic bandwidth compressor (SHBC) combined with NOPA[45]	27.8	12	1	480−750
NOPA with second harmonic generation (SHG)[91]	27 at 599 nm	12 at 745 nm	<1	480−780
optical parametric amplifier (OPA)[92]	10		4.5	615−985
SHG with group velocity mismatch (GVM)[93]		8.5	20	720−890
Pulse expander pumped by OPA[94]	0.9 at 1045 nm		0.70	1000−1090

[a]Some options for generating a tunable Raman pump, including the bandwidth of Raman pump, the bandwidth of resulting stimulated Raman spectrum, conversion efficiency, and tunable range. Blank boxes indicate unreported data.

https://doi.org/10.1021/acsphyschemau.3c00031
ACS Phys. Chem Au 2024, 4, 1−18

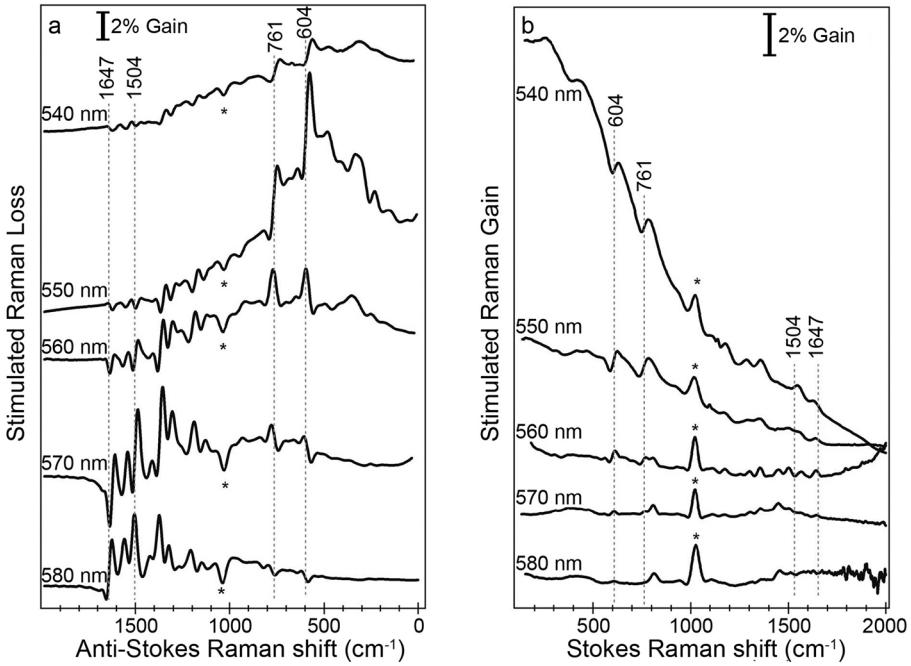

Figure 3. Resonance (a) anti-Stokes and (b) Stokes Raman spectra of rhodamine 6G in methanol at varying pump wavelengths. Solvent peaks are indicated with an asterisk. Adapted with permission from ref 53. Copyright 2008 AIP Publishing.

stimulated Raman signal is maximized, the actinic pump is aligned.

There are several options for maximizing the overlap between the actinic pump and the probe. These include sum frequency generation in a mixing crystal, transient absorption signatures in a well-studied sample, impulsive Raman signal generation in a highly polarizable solvent, or optical Kerr effect cross-correlation (OKE-XC). Most FSRS groups opt for using OKE-XC because it is highly generalizable to many sample conditions and is free from electronic resonance effects. Locating the "time zero," or the delay stage position where the actinic pump and probe have maximum temporal overlap, for a FSRS experiment involves measuring the OKE-XC between the Raman probe and the actinic pump. It is important to carefully select the medium in which the OKE-XC is measured—it should be performed with a material with a large Kerr constant, similar phase and thickness to that of the sample, and one that will not absorb any of the laser pulses. Performing the OKE-XC in, for example, cyclohexane in a 2 mm cuvette and then performing FSRS measurements in a 100 nm thick crystalline sample will likely result in an offset time zero. The two media have different thicknesses and refractive indices, which could alter the time zero position between the FSRS experiment and the OKE-XC measurement.

In an OKE-XC measurement, the spatial and temporal overlap of the actinic pump and probe pulses is measured by the pump-induced change in the polarization of the probe pulse. Lock-in amplification is generally used, as the signals can be quite small. An OKE-XC measurement gives two useful pieces of information: (1) the actinic delay stage position of maximum temporal overlap and (2) the cross-correlation time of the actinic pump and probe pulse. Generally, it is best to minimize the cross-correlation time by appropriate compression of both beams, and wavelength-resolved OKE-XC measurements are helpful to identify higher-order chirp processes impacting the cross-correlation. Common experimental issues when setting up an OKE-XC experiment include using inappropriate polarization conditions, using actinic pump pulses that are too weak, using inappropriately aligned delay stages that translate the beam when moving long distances, or using a noisy probe pulse.

2.4. Data Acquisition

In this section, we discuss the considerations of FSRS data acquisition, including factors to consider for detection and high-duty-cycle data collection. Since excited-state FSRS signals are generally small, with Raman gain values in the range of 0.001−1%, optimization of the SNR is important for a FSRS experiment.

In order to take advantage of the broadband spectral generation, most FSRS experiments involve an array detector, either a photodiode array[3,29,53,75,76,97,101] or a charge-coupled device (CCD) detector.[1,6,16,19,21−25,43,48,50,51,57,59,62,67,68,102−104] Given that FSRS involves detection of small changes on top of the large probe beam background, the well depth and read rates are inherently important factors. Marx and co-workers published an overview of multichannel detectors suitable for FSRS nearly a decade ago, and they described the ideal multichannel detector for FSRS as having high quantum efficiency, enough pixels for sufficient spectral breadth and resolution, high photocurrent per pixel, and high readout rate.[105] Photodiode arrays were used in early FSRS experiments[3,97] because of their large, full well depth, but older technologies had slow read rates, and current technologies can be noisier and are less readily available in complete packages.[38] Thus, FSRS has been performed predominantly with CCDs in recent years,[6,23,24,57,67,104] although the drawbacks of limited well depth and readout rates can be problematic for some applications, along with the high cost for scientific-grade CCDs. They have the advantage of easy operation, very high sensitivity, and low noise and tend to have high readout rates that can allow for single-shot detection at a 1 kHz repetition rate. Single-shot acquisition is an advantage because of the

https://doi.org/10.1021/acsphyschemau.3c00031
ACS Phys. Chem Au 2024, 4, 1−18

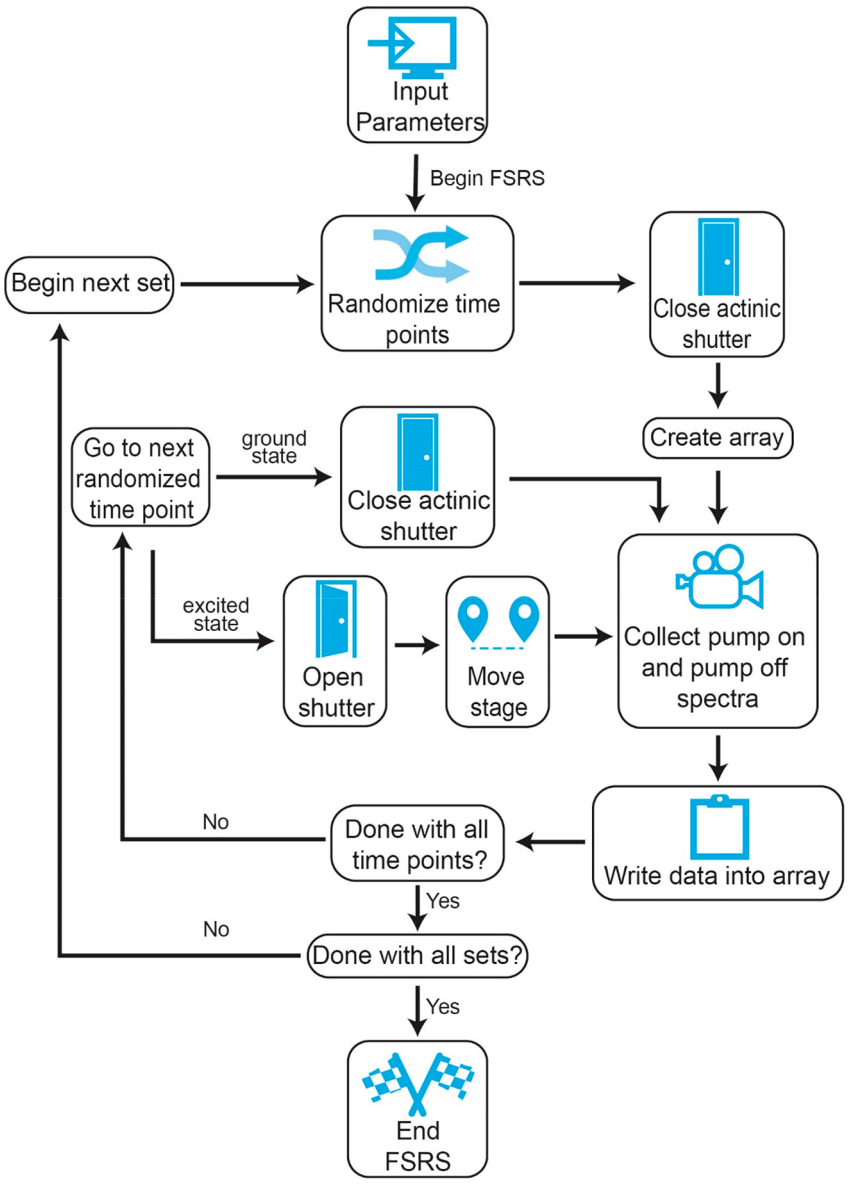

Figure 4. Schematic of how our group's LabView code proceeds to run a FSRS experiment.

ability to record one FSRS spectrum in 2 ms at a 1 kHz repetition rate (1 pump-on spectrum and 1 pump-off spectrum). It is also possible to perform single-shot detection with a photodiode array.[58]

Some more advanced innovations have been made to data acquisition, like using a scanning multichannel technique (SMT) with FSRS.[56,57,106] Briefly, this technique averages spectra collected at different positions of the spectrograph to remove noise caused from variations in pixel-to-pixel sensitivity and noise.[107] Using this frequency-modulated FSRS technique, researchers were able to decrease the smallest resolvable Raman gain from $\sim 1 \times 10^{-4}$ using conventional data processing to $\sim 2 \times 10^{-5}$ by removing pixel-to-pixel nonlinearities and increasing the resultant SNR.

The workflow of a FSRS experiment is also important to consider, particularly in terms of minimizing experiment time and mitigating any photodamage or other sample damage concerns. Here, we describe the workflow for a typical FSRS experiment involving a 1 kHz laser with single shot detection, which generally takes time on the order of 1 h to run.

FSRS spectra are reported with an intensity of stimulated Raman gain, which describes the likelihood of the Raman pump and probe to drive a stimulated Raman transition. These features appear as peaks on top of the broad and intense probe spectrum. Thus, FSRS experiments are run with the Raman pump modulated at half the detector readout rate so that the Raman gain spectrum may be calculated by dividing subsequent acquisitions. For single-shot detection, it is, thus, important to ensure that the detector is triggered at 1 kHz but with a known phase of the Raman pump modulation. To ensure precise timing and synchronization between the laser pulse, detector, and chopper modulating the Raman pump, we employ a D-type flip-flop circuit. The flip-flop circuit is triggered by the 1 kHz laser repetition rate of the laser and the 500 Hz Raman pump chopper, which allows us to collect Raman pump-on and Raman pump-off spectra. To acquire stimulated Raman spectra without photoexcitation, which we call the ground state, we use an automated shutter to block the actinic pump beam. A method of modulating the actinic pump

https://doi.org/10.1021/acsphyschemau.3c00031
ACS Phys. Chem Au 2024, 4, 1−18

Table 3. Raman Differential Scattering Cross Sections of Common Stimulated Raman Standards

molecule	mode (cm^{-1})	excitation wavelength (nm)	Raman cross section (cm^2/molecule·sr)	reference
β-carotene	1520	514	2.04×10^{-24}	114
benzene	992	488	3.65×10^{-29}	115
crystal violet	1620	568	6.75×10^{-25}	116
cyclohexane	802	514	8.29×10^{-30}	117
Nile blue	595	633	4.7×10^{-24}	118
rhodamine 6G	604	532	4.1×10^{-23}	119
3,3′- diethylthiatricarbocyanine	1281	800	1.51×10^{-24}	120

during data collection to perform "active" background subtraction has also been previously presented.[57]

We run our instrumentation and data collection using a master LabView virtual instrument (VI).[108] Each acquisition is run in burst mode, in which acquisitions are stored in the computer random access memory (RAM). We acquire several thousand spectra, then average all the Raman pump-on and Raman pump-off spectra together and write them to the hard drive. This enables single-shot acquisition on a conventional computer and also dramatically reduces the total file size of a FSRS experiment. We find that averaging several thousand spectra at once is ideal because it is fast enough to track any changes in sample condition while resulting in manageable data sets.

The order at which a FSRS experiment proceeds is described here and depicted in Figure 4. The input parameters that must be updated for each FSRS experiment include the list of time delays, the number of acquisitions per saved spectrum, the number of sets (equivalent to how many times to iterate through each time delay), number of ground-state spectrum to collect per set, the file storage location, filename, and time zero position of the delay stage. Some of these factors, like choice of time delay, numbers of images per frame, and number of sets, require careful consideration. The list of time delays should include some negative times (i.e., when the actinic pump arrives at the sample after the Raman pump and probe pair). This will ensure that dynamics induced by the actinic pump can be separated from other nonlinear processes seen in the FSR spectra. It is also important to include many time points close to zero, both positive and negative, in order to track initial dynamics. The time zero position may shift slightly because of differences in thickness or refractive index in the FSRS sample compared with the sample in which the OKE-XC was performed, so including negative time points ensures all dynamics are captured. The number of images per frame should be chosen on the basis of the SNR in the ground-state spectrum. The vibrational peaks should be clearly resolved from the baseline, but using too many images can lead to longer FSRS scans with a higher probability of damaging the sample.

For a typical FSRS scan reported in a publication, each time point is the result of ∼1−100 s of total averaging. For most samples, we find it best to both randomize the time points and cycle through the randomized time points a number of times. This avoids any sample damage bias in the experiment and best accommodates any temporary issues with the experiment, such as bubbles in a flow jet. We find that ∼10 sets is reasonable for most samples, although this will depend on the Raman cross sections, sample optical density, and the likelihood of the sample to be damaged by the laser beams. We also take several ground-state spectra in each set, evenly interspersed throughout the excited-state spectra, in order to monitor any changes to the sample, as well as to provide a high-SNR ground-state spectrum for data analysis.

2.4.1. Additional Directions for FSRS Data Acquisition. FSRS data acquisition has the potential for improvement. Most FSRS experiments have been performed on samples with large Raman cross sections, and extending the technique to less polarizable vibrations would be extremely useful. Also, since high laser flux is often required for FSRS, sample damage over the course of a FSRS scan can be challenging, particularly in samples that require a lot of signal averaging or in our group's recently developed method of spatially offset FSRS (SO-FSRS).[41] Methods of data acquisition that can improve the SNR or decrease the duration of a FSRS scan are beneficial, and some recent advances are encouraging in this regard.

One approach to improve the readout rates and signal-to-noise levels of FSRS experiments involves single-channel detection of a broadband spectrum. Dobner and Fallnich recently demonstrated dispersive Fourier transformation FSRS as a method to overcome the inherent time limitations of common spectrometers used in FSRS experiments.[109] Dispersive Fourier transformation is a method used to acquire a spectrum of one laser pulse by temporally dispersing the signal, thereby allowing each frequency component to be resolved by a single fast photodiode.[110] Their method allowed the collection of one Raman spectrum in 2 μs with 20 averages achieving SNR comparable with a CCD reading.[109] While recent developments in dispersive Fourier transformation methods have been discussed at length elsewhere,[110] this field holds promise for decreasing acquisition times for FSRS.

Compressive sensing approaches can also be used to reduce the total duration of a FSRS experiment. Similar to compressive sensing implementations in two-dimensional infrared (2D-IR) spectroscopy[111] and TA spectroscopy,[112] FSRS-based compressive sensing relies on reduction of the individual time point spectra to reconstruct the full transient dynamics. Using this knowledge, researchers can collect fewer measurements and still retain good SNR. In practice, this reduces the experiment time by a factor of about 2, given sufficient prior knowledge of the dynamics. This could clearly be useful for FSRS experiments that require lots of signal averaging and time delays or for samples that readily photodamage under the high flux of ultrafast lasers. More advanced compressive sensing methods hold promise for spectroscopy, such as FSRS, but have yet to be implemented.

2.5. Sample Considerations

There are several aspects to consider when choosing a molecular system to study with FSRS. A key factor is the Raman cross section, as this dictates the signal magnitude.[113] In Table 3, we list the Raman differential scattering cross section of a series of molecules commonly used for FSRS alignment or technique development. These molecules have

https://doi.org/10.1021/acsphyschemau.3c00031
ACS Phys. Chem Au 2024, 4, 1−18

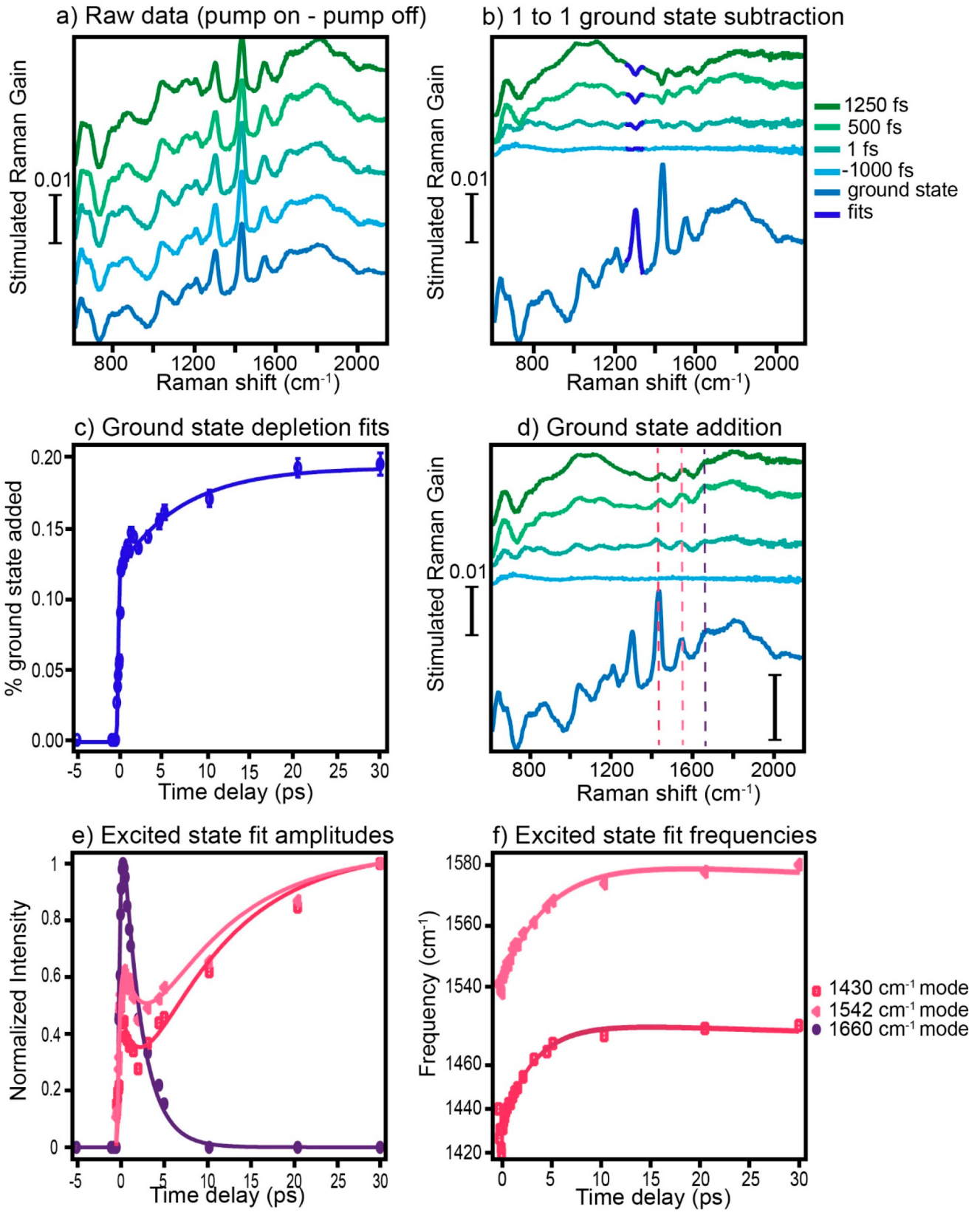

Figure 5. A step-by-step process of standard FSRS data analysis methods, as shown for a crystalline rubrene sample. (a) Raw FSRS data with a total acquisition time of 20−90 s per time point, followed by (b) one-to-one ground-state subtraction. The ground-state depletion is fit at each time delay (dark blue overlay) and used to determine (c) the amount of ground state to add back to each excited-state spectrum. (d) Spectrum after ground-state addition shows only excited-state contributions, which can be fit to examine dynamics, such as (e) amplitude and (f) frequencies, over time following photoexcitation. Adapted with permission from ref 16. Copyright 2017 American Chemical Society.

https://doi.org/10.1021/acsphyschemau.3c00031
ACS Phys. Chem Au 2024, 4, 1−18

conjugated polyenes and aromatic rings and are, therefore, highly polarizable. However, FSRS measurements have been performed on samples with much lower Raman cross sections than these, and preresonant enhancement can be quite beneficial for many systems.

For most transmission-based FSRS experiments, it is ideal if the optical density, equivalent to absorbance per path length, of the sample at the actinic pump wavelength is around 1.0. At lower optical densities, there are fewer molecules to provide a Raman signal. At higher optical densities, the actinic pump pulse will not penetrate well to the back face of the sample, which means that only a small portion of the measured molecules will be photoexcited. Thus, an optical density in the range 0.7−1.2 is generally optimal. Additionally, the sample should have low or no absorbance in the probe's spectral region to avoid losing signal magnitude to probe absorption in the resulting FSRS spectra. In some cases, when samples have high optical densities or when investigating nontransmissive samples, FSRS can be measured in a reflective geometry rather than transmissive.[23]

Sample damage can be an issue in ultrafast spectroscopy, particularly for biological samples, because of the high peak intensity of the short laser pulses used. For example, for a beam that has a 1 kHz repetition rate, 200 μW average power, 100 fs pulse width, and is focused to 10 μm diameter, the peak power is 2 MW, and the peak flux is 25 TW/cm^2, which is more than capable of damaging most samples. For FSRS, it is crucial to ensure that any signals observed are representative of the photochemistry of interest and not the result of sample degradation over time. A simple way to look for sample damage is to look at the ground-state Raman gain of the sample over time. By performing this experiment with varying beam powers and exposure time, we can determine the threshold power to initiate sample damage and also the critical time the sample can withstand under the exposure of the particular laser. Typically, we set a threshold after which we discard data. For example, once the ground-state signal is reduced to 80% of the first ground-state spectrum, we discard all data collected after that point. This allows us to ensure that the majority of the signals we observe are not the result of photodamage.

There are several methods to reduce sample damage. With solution phase measurements, the best way to minimize sample damage is to use a flow cell setup or a cuvette with a stir bar to agitate the sample and ensure molecules do not spend too much time in the laser path. The flow cell demonstrates the most sample longevity, but this can present issues if the volume of the sample is too small. For small sample volumes, stirring with a microstir bar presents the next best choice. Solid samples can be mounted over a spinning stage[121] or raster-scanned during data collection to reduce the amount of time a specific region spends in the laser path. Sealing solid samples inside epoxy or superglue or using a nitrogen atmosphere helps to prevent oxidation and delay sample damage, as well.

For anisotropic samples, such as crystals, the relative orientation of the crystal axes and the laser polarization are also an important experimental factor. While the Raman pump and probe beams are parallel to each other, their orientation to the axes of a crystal's unit cell can change the relative intensities of Raman modes measured.[23] FSRS is typically used to measure early time dynamics where rotational anisotropy is generally not a factor, and so, the actinic pump is usually parallel to the Raman pump and probe to maximize the excited-state signal. The intensity of Raman signal in solids is highly dependent on crystalline orientation and the polarization of the incoming laser, and different transition dipole moments can be accessed using different polarization conditions.[122−124] Our group's recent work built on this concept to observe rates of forward and back electron transfer in betaine-30 crystals using different polarizations of the pump and probe beams relative to the crystal axes.[23] Therefore, polarization conditions should be considered carefully during FSRS experiments.

2.6. Data Analysis Methods

In this section, we describe the basic analyses performed on the FSRS data, followed by a discussion of more advanced data analysis techniques. We perform most of our data analysis in Igor Pro, Matlab, and increasingly in Python. We first average all of the spectra corresponding to the same time point together and subtract the averaged ground-state spectrum from each of these time points. This one-to-one subtraction is important because it removes any ground-state contributions, in addition to systemic noise. Following one-to-one subtraction, noise levels can be reduced by about an order of magnitude from around $1-10 \times 10^{-3}$ counts in raw spectra to 1×10^{-4} counts. In a typical experiment, we find that the SNR in one-to-one subtracted spectra is approximately 1−10, although this will vary on the basis of the molecule's Raman cross section, magnitude of excited-state signals, and detector sensitivity. Typically, one-to-one subtraction results in negative features at ground-state frequencies because of the bleach of the ground state (Figure 5b). Changes to solvent peak intensities following one-to-one subtraction can indicate a change in the resonance condition of the analyte and can also be used to monitor the excited-state dynamics.

The FSRS process also gives TA information and can give rise to broad four-wave mixing peaks, which can present as background. Generally, we fit this background to a polynomial function and subtract it. However, if there are negative or dispersive features in the femtosecond stimulated Raman spectra, background subtraction can introduce artifacts and should be done carefully, and each subtraction should be examined manually.

Because of the fact that some of the sample should be in an electronic excited state for much of the FSRS data set, the one-to-one subtraction results in negative ground-state Raman features. We examine the amplitudes for these bleach features (Figure 5b) and add back in a portion of the ground-state spectrum in order to visualize any transient excited-state features. For most samples, the amplitude of this depletion over time should increase sharply at time zero, as the ground-state is depopulated, and then gradually decrease as the ground state is repopulated at later time delays. We typically calculate the percent ground-state depletion at each excited-state time (Figure 5c) and then add back this portion of the ground state to each excited-state spectrum. Occasionally, it is better to add back portions of a fitted ground-state spectrum so as to not introduce additional noise. By adding back a small amount of the ground state, excited-state features are clearer without the large ground-state depletion signals there to obscure small excited-state peaks and frequency shifts (Figure 5d).

Finally, we fit excited-state peaks and examine how excited-state vibrational properties, like amplitude (Figure 5e) and frequency (Figure 5f), evolve over time. We use this information to extract information on dynamics in the system

https://doi.org/10.1021/acsphyschemau.3c00031
ACS Phys. Chem Au 2024, 4, 1−18

under study. We also must convolute the OKE-XC with the kinetic data to extract useful information (Figure 5e) and to account for growth of the signal at short time delays that are the result of the temporal shape of the OKE-XC versus time-resolved photobleaching or excited-state signal.

2.6.1. Advanced Analyses. FSRS is not immune to spectral artifacts and features arising from other nonlinear optical processes that can limit the ability to discriminate Raman features. These signals are often sample-dependent, which arises from other nonlinear optical processes occurring in the material, such as TA, stimulated emission, XPM, and OKE. For FSRS spectra, distinguishing Raman features from non-Raman spectral features can present some challenges. It is important to note, however, that this problem arises in most nonlinear and ultrafast spectroscopic experiments, and as a result, there are a host of methods to help overcome these limitations through data analysis techniques or experimental design principles. In most cases, the success of these techniques depends on the SNR of the Raman peaks compared with those of other spectral features.

A particularly useful method for discriminating Raman peaks relative to broad background signals is to take the derivative of the FSRS spectrum with respect to frequency.[49] For most cases, because vibrational lifetimes are considerably longer than electronic responses, Raman peaks are spectrally narrower than those of other optical features. As a result, taking the derivative of a FSR spectrum will produce sharp dispersive line shapes for Raman modes, while broader features will generally be relegated to the background (Figure 6). In fact, Kloz et al. have developed a method to explicitly detect the first derivative of a FSRS signal rather than the more traditional detection scheme.[55]

This approach has a few useful benefits, with one being that unlike many baseline subtraction algorithms, one can find both positive and negative Raman peaks. Moreover, in particularly crowded spectra where peaks can emerge as shoulders of stronger peaks, the derivative spectrum can often effectively distinguish these shoulders because of its sensitivity to inflection points. In Figure 6a, we show the stimulated Raman spectrum of tetra(sulfonatophenyl)porphyrin (TSPP), followed by the first derivative (Figure 6b) of the same spectrum. The background of the first derivative was fit and then removed from the fitted vibrational spectrum, which resulted in a clean fit with no background noise and clear vibrational peaks (Figure 6c).

The derivative approach is limited by its reliance on high SNR and the assumption that Raman modes are significantly more spectrally narrow than other spectral features. In the case where signal-to-noise is weak and Raman features are difficult to distinguish from non-Raman features, an alternative is to use matrix decomposition methods like singular value decomposition (SVD).[126,127] This decomposition method allows the user to distinguish signals on the basis of common variance and is often useful to distinguish spectral features that exhibit similar dynamics. This can be particularly useful in instances where large oscillatory backgrounds arise from XPM. SVD can separate this effect as a separate component from other spectral components with unique dynamics.

Figure 7 shows the one-to-one ground-state-subtracted FSRS spectra (Figure 7a) of TSPP aggregates, where the 1530 and 1540 cm^{-1} mode ground-state depletion is obscured by the noise in comparison with the same data set in which the first component of SVD is applied (Figure 7b). The ground-

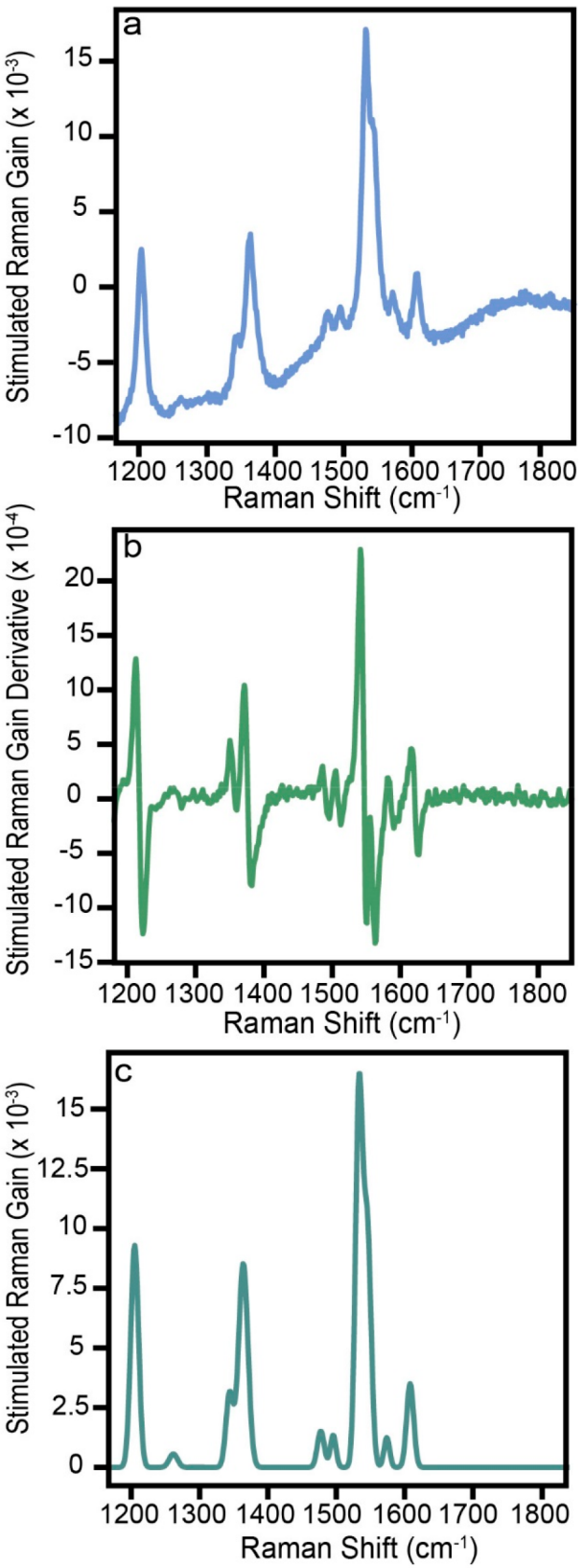

Figure 6. (a) Raw stimulated Raman spectrum of tetrasulfonatophenylporphyrin aggregates and (b) the first derivative of the data. (c) Fitted vibrational spectrum with background obtained from the first derivative spectrum subtracted out. Adapted with permission from ref 125. Copyright 2021 American Chemical Society.

https://doi.org/10.1021/acsphyschemau.3c00031
ACS Phys. Chem Au 2024, 4, 1−18

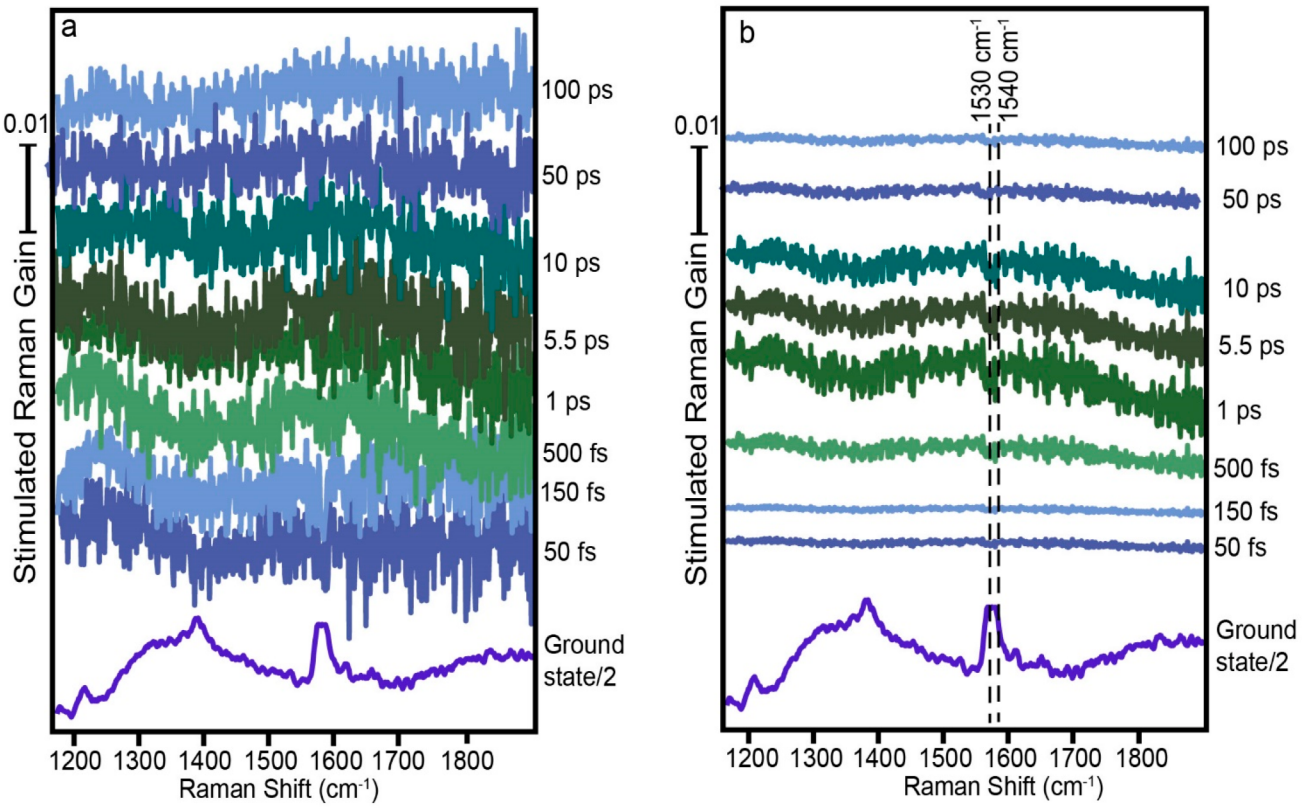

Figure 7. (a) One-to-one ground-state-subtracted data set and (b) spectra after applying SVD, which can pull out vibrational dynamics over the noise. The data set measures the weak dynamics of depolarized femtosecond stimulated Raman scattering of tetra(sulfonatophenyl)porphyrin aggregates. Adapted with permission from ref 125. Copyright 2021 American Chemical Society.

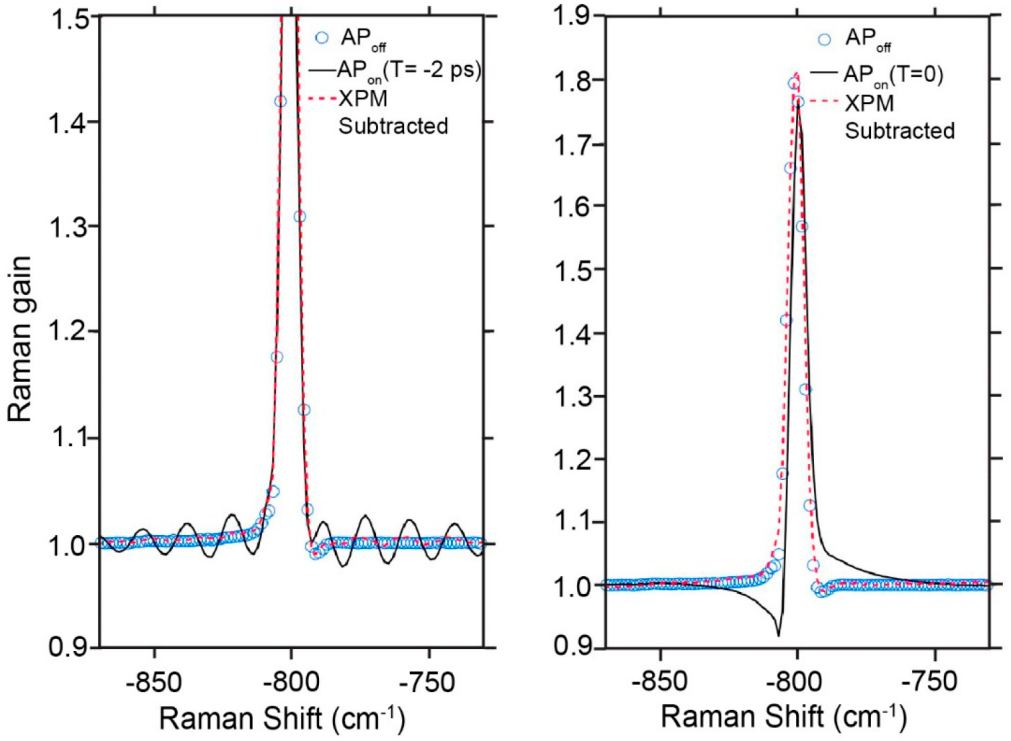

Figure 8. FSRS spectra of cyclohexane measured without (blue) and with (black) the actinic pump pulse, with a reconstructed spectrum (red) obtained by subtracting the calculated XPM signal. Right panel at $T = -2$ ps, and left panel at $T = 0$ ps. Adapted with permission from ref 51. Copyright 2019 American Chemical Society.

https://doi.org/10.1021/acsphyschemau.3c00031
ACS Phys. Chem Au 2024, 4, 1−18

state depletion of the 1530 and 1540 cm^{-1} modes is clearer, which highlights the SVD's ability to pull out dynamics specific to the vibrational spectrum rather than the noise. In addition to separating Raman spectral features from other optical responses, this method also gives the user the ability to separate out spectral features, which undergo unique dynamics to produce decay-associated spectra in a similar strategy to that typically applied to TA measurements.

For data sets with strong XPM background signals, Batignani and co-workers recently outlined a method for distinguishing XPM and genuine dynamics in FSRS spectra by identifying the origin of XPM signals and subsequently removing them from spectra of interest.[51] This method involves fitting XPM signals that occur at negative time points, where there are no photoinduced processes at play, and using the parameters to calculate the XPM-induced signals at early time delays (Figure 8). Then, the XPM can be subtracted from the spectra, thereby distinguishing XPM artifacts from photoinduced dynamics.

In a unique implementation of FSRS that integrates a facile pulse-shaping technique, Kloz and co-workers introduced a custom optical chopper in the Fourier plane of their grating filter to produce their Raman pump pulses that were frequency-modulated to periodically adjust the Raman pump central frequency and bandwidth.[55] This methodology produced effective first-derivative spectra that, for reasons similar to those described above, emphasize the typically sharp, spectrally narrow Raman features over broader non-Raman spectral features. A publication by Bera and co-workers introduced another approach to this method of shaping the Raman pump through simultaneous generation of two spectrally distinct Raman pump pulses, which leveraged the Raman pump frequency dependence that is exclusive to Raman scattering.[83]

Additionally, Kloz and co-workers included a further step to their baseline subtraction that included Fourier filtration to separate their derivative Raman features from higher-frequency noise and baseline artifacts, which proved effective. Fourier filtering involves the sorting of bins of data through fast Fourier transform (often sorted by the frequency of various features), followed by a windowing step, which filters out the undesired spectral features from the Raman components. This Fourier filtering process can be simply coded in MatLab and Python coding architectures and can be used both on the derivative Raman spectra described above and on conventional Raman spectra, particularly when the filtering of oscillatory background features is desired.

More recently, machine learning (ML) techniques have been adopted to aid in Raman data analysis. ML algorithms are able to learn and make predictions without being explicitly programmed and have some advantages over traditional chemometric analyses, like the ability to efficiently analyze large data sets and identify complex patterns.[128] A recent study demonstrated the use of a deep-learning model, a type of ML where algorithms create a network to store data and to learn, to denoise mass data sets. Researchers have demonstrated both supervised and unsupervised deep-learning algorithms, whereby a supervised approach requires high-quality data for training, and unsupervised techniques can be trained with noisier data.[129] The different approaches improved denoising by 50% and 36%, respectively, when compared with traditional denoising techniques, like fast Fourier transform filters.[129] ML algorithms like this have the potential to improve FSRS data analysis and enable researchers to uncover crucial information in noisy data sets, which could open the door to studying materials with less signal averaging or with lower Raman scattering cross sections.

4. OUTLOOK

In this review, we have outlined some important factors for building and operating a FSRS instrument, including beam generation, sample considerations, and data analysis. Current FSRS techniques are powerful in revealing crucial ultrafast structural dynamics, and new advances in the field continue to demonstrate its utility. FSRS is an evolving field with novel technique developments, like surface-enhanced FSRS (SE-FSRS),[130,131] SO-FSRS,[41] coherent control,[42] anti-Stokes FSRS,[27] and more. These techniques open the door to exploring new questions and building a deeper understanding of ultrafast phenomena.

Our group recently presented a novel technique, SO-FSRS, which probes how vibrational motions are coupled to excited-state transport on micron-length scales.[41] Analogous to transient absorption microscopy (TAM) but with additional vibrational information, the SO-FSRS uses galvanic scanning mirrors to spatially offset the actinic pump from the Raman pump and probe. The actinic pump is raster-scanned across a sample, while the Raman pump and probe remain stationary. We perform a complete FSRS scan at each spatially offset actinic pump position and observe how the excited-state structure evolves as a function of both time and location following photoexcitation. This technique facilitates a new understanding of how molecular and crystal structure drive photoexcited phenomena in solid-state samples.

Advances in optical pulse shaping in recent decades have opened the door to coherent control experiments, where a double-pulse scheme selectively excites specific vibrations in a molecular system.[42,132−136] Coherent control has the ability to selectively drive molecular interactions, like activating specific phase transitions[133] and even bond formation.[136] While coherent control has been applied to some Raman spectroscopy techniques,[137,138] it has only recently been applied to FSRS.[42] Coherent control of FSRS can uncover coupling between inter- and intramolecular vibrations, reveal which lattice phonon vibrations drive or impede photophysical phenomena, and provide greater insight in the design of novel materials. The ability to selectively amplify and damp specific lattice vibrations during photoexcitation and then observe the resulting structural dynamics allows for greater manipulation of photoinduced processes and promotes a deeper understanding of the roles of molecular and crystal structures in ultrafast photophysical dynamics.

Another novel technique receiving a great deal of attention in the literature is the use of entangled photons in nonlinear spectroscopy. Nearly a decade ago, Mukamel and co-workers proposed using entangled photons in FSRS experiments.[139] In their proposed method, the Raman probe would be replaced with a pair of broadband entangled photons. One photon interacts with the sample with a third narrowband pulse (Raman pump) in which the second entangled photon acts as a reference and does not interact with the sample. This method provides several advantages over traditional FSRS experiments, like reducing SNR and allowing for the use of lower-intensity laser light, which can reduce sample damage.[139] Other theoretical calculations have demonstrated that using entangled photons can selectively enhance or suppress SRS signals.[140] Recently, researchers presented a quantum exten-

https://doi.org/10.1021/acsphyschemau.3c00031
ACS Phys. Chem Au 2024, 4, 1−18

sion of FSRS called quantum femtosecond Raman spectroscopy (QFRS) that replaces a narrowband probe pulse with a broadband pair of entangled photons, which allows for higher temporal resolution without sacrificing spectral resolution and could increase the resonance enhancement by up to 4 times without the need for higher laser powers.[141] While entangled FSRS has yet to be experimentally realized, the use of lower fluxes in these measurements is quite appealing, as is the possibility of interrogating quantum phenomena while using quantum light.

FSRS has the unique ability to track structural changes in electronic excited states and has answered key questions for applications in renewable energy,[14,104] bioimaging,[6] phototherapy,[142] and beyond. New advances in ML techniques for data analysis, as well as the promise of quantum-enhanced FSRS on the horizon, demonstrate the future ability of FSRS to investigate samples with smaller cross sections, thereby opening the door even wider for molecular systems that can be investigated. Recent developments in coherent control FSRS show exceptional potential in controlling site-specific chemistry and realizing the long-held promise of the selective control of individual bonds. With these advances, FSRS continues to pave the way for novel insights into ultrafast phenomena. Moving forward, we hope this practical guide will help researchers implement their own FSRS experiments and drive the field to even more innovative research directions.

AUTHOR INFORMATION

Corresponding Author

Renee R. Frontiera − *Department of Chemistry, University of Minnesota, Minneapolis, Minnesota 55455, United States;* orcid.org/0000-0001-8218-7574; Email: rrf@umn.edu

Authors

Pauline G. Lynch − *Department of Chemistry, University of Minnesota, Minneapolis, Minnesota 55455, United States*

Aritra Das − *Department of Chemistry, University of Minnesota, Minneapolis, Minnesota 55455, United States*

Shahzad Alam − *Department of Chemistry, University of Minnesota, Minneapolis, Minnesota 55455, United States*

Christopher C. Rich − *Department of Chemistry, University of Minnesota, Minneapolis, Minnesota 55455, United States;* Present Address: Binghamton University, Department of Chemistry, Binghamton, New York 13902, United States

Complete contact information is available at: https://pubs.acs.org/10.1021/acsphyschemau.3c00031

Author Contributions

CRediT: **Pauline G. Lynch** writing-original draft, writing-review & editing; **Aritra Das** writing-original draft; **Shahzad Alam** writing-original draft; **Christopher C. Rich** writing-original draft; **Renee R. Frontiera** funding acquisition, project administration, writing-original draft, writing-review & editing.

Notes

The authors declare no competing financial interest.

ACKNOWLEDGMENTS

This work is supported by Department of Energy DE-SC-0023374.

REFERENCES

(1) Yoshizawa, M.; Aoki, H.; Hashimoto, H. Vibrational Relaxation of the $2A_g^-$ Excited State in All-Trans-Beta-Carotene Obtained by Femtosecond Time-Resolved Raman Spectroscopy. *Phys. Rev. B* **2001**, *63* (18), 180301.

(2) McCamant, D. W.; Kim, J. E.; Mathies, R. A. Vibrational Relaxation in β-Carotene Probed by Picosecond Stokes and Anti-Stokes Resonance Raman Spectroscopy. *J. Phys. Chem. A* **2002**, *106* (25), 6030−6038.

(3) McCamant, D. W.; Kukura, P.; Mathies, R. A. Femtosecond Broadband Stimulated Raman: A New Approach for High-Performance Vibrational Spectroscopy. *Appl. Spectrosc.* **2003**, *57* (11), 1317−1323.

(4) McCamant, D. W. Femtosecond Stimulated Raman Spectroscopy of Ultrafast Biophysical Reaction Dynamics. Ph.D. Dissertation, University of California, Berkeley, CA, 1995. https://www.proquest.com/docview/305211983/abstract/4FCFD474FB724082PQ/1 (accessed 2023-06-25).

(5) *Google Scholar*. https://scholar.google.com/scholar?hl=en&as_sdt=0%2C24&q=%22femtosecond+stimulated+raman%22&btnG= (accessed 2023-06-25).

(6) Wei, J.; Wu, Y.; Pu, R.; Shi, L.; Jiang, J.; Du, J.; Guo, Z.; Huang, Y.; Liu, W. Tracking Ultrafast Structural Dynamics in a Dual-Emission Anti-Kasha-Active Fluorophore Using Femtosecond Stimulated Raman Spectroscopy. *J. Phys. Chem. Lett.* **2021**, *12*, 4466.

(7) McCamant, D. W.; Kukura, P.; Mathies, R. A. Femtosecond Time-Resolved Stimulated Raman Spectroscopy: Application to the Ultrafast Internal Conversion in β-Carotene. *J. Phys. Chem. A* **2003**, *107* (40), 8208−8214.

(8) Fröbel, S.; Buschhaus, L.; Villnow, T.; Weingart, O.; Gilch, P. The Photoformation of a Phthalide: A Ketene Intermediate Traced by FSRS. *Phys. Chem. Chem. Phys.* **2015**, *17* (1), 376−386.

(9) Pontecorvo, E.; Ferrante, C.; Elles, C. G.; Scopigno, T. Structural Rearrangement Accompanying the Ultrafast Electrocyclization Reaction of a Photochromic Molecular Switch. *J. Phys. Chem. B* **2014**, *118* (24), 6915−6921.

(10) Farrow, G. A.; Quick, M.; Kovalenko, S. A.; Wu, G.; Sadler, A.; Chekulaev, D.; Chauvet, A. A. P.; Weinstein, J. A.; Ernsting, N. P. On the Intersystem Crossing Rate in a Platinum(II) Donor-Bridge-Acceptor Triad. *Phys. Chem. Chem. Phys.* **2021**, *23* (38), 21652−21663.

(11) Yoon, S.; Kukura, P.; Stuart, C. M.; Mathies, R. A. Direct Observation of the Ultrafast Intersystem Crossing in Tris(2,2′-Bipyridine)Ruthenium(II) Using Femtosecond Stimulated Raman Spectroscopy. *Mol. Phys.* **2006**, *104* (8), 1275−1282.

(12) Hall, C. R.; Romanov, A. S.; Bochmann, M.; Meech, S. R. Ultrafast Structure and Dynamics in the Thermally Activated Delayed Fluorescence of a Carbene-Metal-Amide. *J. Phys. Chem. Lett.* **2018**, *9* (19), 5873−5876.

(13) Hart, S. M.; Silva, W. R.; Frontiera, R. R. Femtosecond Stimulated Raman Evidence for Charge-Transfer Character in Pentacene Singlet Fission. *Chem. Sci.* **2018**, *9* (5), 1242−1250.

(14) Bera, K.; Douglas, C. J.; Frontiera, R. R. Femtosecond Stimulated Raman Spectroscopy-Guided Library Mining Leads to Efficient Singlet Fission in Rubrene Derivatives. *Chem. Sci.* **2021**, *12*, 13825−13835.

(15) Schultz, J. D.; Shin, J. Y.; Chen, M.; O'Connor, J. P.; Young, R. M.; Ratner, M. A.; Wasielewski, M. R. Influence of Vibronic Coupling on Ultrafast Singlet Fission in a Linear Terrylenediimide Dimer. *J. Am. Chem. Soc.* **2021**, *143* (4), 2049−2058.

(16) Bera, K.; Douglas, C. J.; Frontiera, R. R. Femtosecond Raman Microscopy Reveals Structural Dynamics Leading to Triplet Separation in Rubrene Singlet Fission. *J. Phys. Chem. Lett.* **2017**, *8* (23), 5929−5934.

(17) Bera, K.; Kwang, S. Y.; Frontiera, R. R. Advances in Singlet Fission Chromophore Design Enabled by Vibrational Spectroscopies. *J. Phys. Chem. C* **2020**, *124* (46), 25163−25174.

(18) Young, R. M.; Dyar, S. M.; Barnes, J. C.; Juríček, M.; Stoddart, J. F.; Co, D. T.; Wasielewski, M. R. Ultrafast Conformational

Dynamics of Electron Transfer in ExBox^{4+}⊂Perylene. *J. Phys. Chem. A* **2013**, *117* (47), 12438−12448.
(19) Frontiera, R. R.; Dasgupta, J.; Mathies, R. A. Probing Interfacial Electron Transfer in Coumarin 343 Sensitized TiO_2 Nanoparticles with Femtosecond Stimulated Raman. *J. Am. Chem. Soc.* **2009**, *131* (43), 15630−15632.
(20) Ellis, S. R.; Hoffman, D. P.; Park, M.; Mathies, R. A. Difference Bands in Time-Resolved Femtosecond Stimulated Raman Spectra of Photoexcited Intermolecular Electron Transfer from Chloronaphthalene to Tetracyanoethylene. *J. Phys. Chem. A* **2018**, *122*, 3594.
(21) Silva, W. R.; Frontiera, R. R. Excited State Structural Evolution during Charge-Transfer Reactions in Betaine-30. *Phys. Chem. Chem. Phys.* **2016**, *18* (30), 20290−20297.
(22) Frontiera, R. R.; Fang, C.; Dasgupta, J.; Mathies, R. A. Probing Structural Evolution along Multidimensional Reaction Coordinates with Femtosecond Stimulated Raman Spectroscopy. *Phys. Chem. Chem. Phys.* **2012**, *14* (2), 405−414.
(23) Cassabaum, A. A.; Silva, W. R.; Rich, C. C.; Frontiera, R. R. Orientation and Polarization Dependence of Ground- and Excited-State FSRS in Crystalline Betaine-30. *J. Phys. Chem. C* **2019**, *123* (20), 12563−12572.
(24) Boulanger, S. A.; Chen, C.; Myasnyanko, I. N.; Baranov, M. S.; Fang, C. Fluorescence Modulation of Ortho-Green Fluorescent Protein Chromophores Following Ultrafast Proton Transfer in Solution. *J. Phys. Chem. B* **2022**, *126* (27), 5081−5093.
(25) Tang, L.; Liu, W.; Wang, Y.; Zhao, Y.; Oscar, B. G.; Campbell, R. E.; Fang, C. Unraveling Ultrafast Photoinduced Proton Transfer Dynamics in a Fluorescent Protein Biosensor for Ca^{2+} Imaging. *Chem.—Eur. J.* **2015**, *21* (17), 6481−6490.
(26) Fang, C.; Frontiera, R. R.; Tran, R.; Mathies, R. A. Mapping GFP Structure Evolution during Proton Transfer with Femtosecond Raman Spectroscopy. *Nat. Lett.* **2009**, *462* (7270), 200−204.
(27) Liu, W.; Tang, L.; Oscar, B. G.; Wang, Y.; Chen, C.; Fang, C. Tracking Ultrafast Vibrational Cooling during Excited-State Proton Transfer Reaction with Anti-Stokes and Stokes Femtosecond Stimulated Raman Spectroscopy. *J. Phys. Chem. Lett.* **2017**, *8*, 997−1003.
(28) Liu, W.; Han, F.; Smith, C.; Fang, C. Ultrafast Conformational Dynamics of Pyranine during Excited State Proton Transfer in Aqueous Solution Revealed by Femtosecond Stimulated Raman Spectroscopy. *J. Phys. Chem. B* **2012**, *116* (35), 10535−10550.
(29) Kukura, P.; McCamant, D. W.; Yoon, S.; Wandschneider, D. B.; Mathies, R. A. Structural Observation of the Primary Isomerization in Vision with Femtosecond-Stimulated Raman. *Science.* **2005**, *310* (5750), 1006−1009.
(30) Hall, C. R.; Conyard, J.; Heisler, I. A.; Jones, G.; Frost, J.; Browne, W. R.; Feringa, B. L.; Meech, S. R. Ultrafast Dynamics in Light-Driven Molecular Rotary Motors Probed by Femtosecond Stimulated Raman Spectroscopy. *J. Am. Chem. Soc.* **2017**, *139* (21), 7408−7414.
(31) Quick, M.; Dobryakov, A. L.; Ioffe, I. N.; Berndt, F.; Mahrwald, R.; Ernsting, N. P.; Kovalenko, S. A. Rotamer-Specific Photoisomerization of Difluorostilbenes from Transient Absorption and Transient Raman Spectroscopy. *J. Phys. Chem. B* **2018**, *122* (3), 1049−1059.
(32) Wang, Z.; Zhang, Y.; Chen, C.; Zhu, R.; Jiang, J.; Weng, T.-C.; Ji, Q.; Huang, Y.; Fang, C.; Liu, W. Mapping the Complete Photocycle That Powers a Large Stokes Shift Red Fluorescent Protein. *Angew. Chem., Int. Ed.* **2023**, *62* (5), No. e202212209.
(33) Dasgupta, J.; Frontiera, R. R.; Taylor, K. C.; Lagarias, J. C.; Mathies, R. A. Ultrafast Excited-State Isomerization in Phytochrome Revealed by Femtosecond Stimulated Raman Spectroscopy. *Proc. Natl. Acad. Sci. U. S. A.* **2009**, *106* (6), 1784−1789.
(34) Hontani, Y.; Broser, M.; Luck, M.; Weißenborn, J.; Kloz, M.; Hegemann, P.; Kennis, J. T. M. Dual Photoisomerization on Distinct Potential Energy Surfaces in a UV-Absorbing Rhodopsin. *J. Am. Chem. Soc.* **2020**, *142* (26), 11464−11473.
(35) Cassabaum, A. A.; Bera, K.; Rich, C. C.; Nebgen, B. R.; Kwang, S. Y.; Clapham, M. L.; Frontiera, R. R. Femtosecond Stimulated Raman Spectro-Microscopy for Probing Chemical Reaction Dynamics in Solid-State Materials. *J. Chem. Phys.* **2020**, *153* (3), 030901.
(36) McCamant, D. W.; Kukura, P.; Yoon, S.; Mathies, R. A. Femtosecond Broadband Stimulated Raman Spectroscopy: Apparatus and Methods. *Rev. Sci. Instrum.* **2004**, *75* (11), 4971−4980.
(37) Kukura, P.; McCamant, D. W.; Mathies, R. A. Femtosecond Stimulated Raman Spectroscopy. *Annu. Rev. Phys. Chem.* **2007**, *58* (1), 461−488.
(38) Frontiera, R. R.; Mathies, R. A. Femtosecond Stimulated Raman Spectroscopy. *Laser Photonics Rev.* **2011**, *5* (1), 102−113.
(39) Kukura, P.; Yoon, S.; Mathies, R. A. Femtosecond Stimulated Raman Spectroscopy. *Anal. Chem.* **2006**, *78* (17), 5952−5959.
(40) Dietze, D. R.; Mathies, R. A. Femtosecond Stimulated Raman Spectroscopy. *ChemPhysChem* **2016**, *17* (9), 1224−1251.
(41) Kwang, S. Y.; Frontiera, R. R. Spatially Offset Femtosecond Stimulated Raman Spectroscopy: Observing Exciton Transport through a Vibrational Lens. *J. Phys. Chem. Lett.* **2020**, *11* (11), 4337−4344.
(42) Rich, C. C.; Frontiera, R. R. Uncovering the Functional Role of Coherent Phonons during the Photoinduced Phase Transition in a Molecular Crystal. *J. Phys. Chem. Lett.* **2020**, *11*, 7502.
(43) Rondonuwu, F. S.; Watanabe, Y.; Zhang, J.-P.; Furuichi, K.; Koyama, Y. Internal-Conversion and Radiative-Transition Processes among the $1B_u^+$, $1B_u^-$ and $2A_g^-$ States of All-Trans-Neurosporene as Revealed by Subpicosecond Time-Resolved Raman Spectroscopy. *Chem. Phys. Lett.* **2002**, *357* (5), 376−384.
(44) Yoon, S.; Mccamant, D. W.; Kukura, P.; Mathies, R. A.; Zhang, D.; Lee, S.-Y. Dependence of Line Shapes in Femtosecond Broadband Stimulated Raman Spectroscopy on Pump-Probe Time Delay. *J. Chem. Phys.* **2005**, *122*, 24505.
(45) Zhu, L.; Liu, W.; Fang, C. A Versatile Femtosecond Stimulated Raman Spectroscopy Setup with Tunable Pulses in the Visible to near Infrared. *Appl. Phys. Lett.* **2014**, *105*, 041106.
(46) Batignani, G.; Ferrante, C.; Scopigno, T. Accessing Excited State Molecular Vibrations by Femtosecond Stimulated Raman Spectroscopy. *J. Phys. Chem. Lett.* **2020**, *11*, 7805.
(47) Oscar, B. G.; Chen, C.; Liu, W.; Zhu, L.; Fang, C. Dynamic Raman Line Shapes on an Evolving Excited-State Landscape: Insights from Tunable Femtosecond Stimulated Raman Spectroscopy. *J. Phys. Chem. A* **2017**, *121* (29), 5428−5441.
(48) Tang, L.; Zhu, L.; Taylor, M. A.; Wang, Y.; Remington, S. J.; Fang, C. Excited State Structural Evolution of a GFP Single-Site Mutant Tracked by Tunable Femtosecond-Stimulated Raman Spectroscopy. *Molecules* **2018**, *23* (9), 2226.
(49) Frontiera, R. R.; Gruenke, N. L.; Van Duyne, R. P. Fano-like Resonances Arising from Long-Lived Molecule-Plasmon Interactions in Colloidal Nanoantennas. *Nano Lett.* **2012**, *12* (11), 5989−5994.
(50) Chen, C.; Zhu, L.-D.; Fang, C. Femtosecond Stimulated Raman Line Shapes: Dependence on Resonance Conditions of Pump and Probe Pulses. *Chin. J. Chem. Phys.* **2018**, *31* (4), 492−502.
(51) Batignani, G.; Fumero, G.; Pontecorvo, E.; Ferrante, C.; Mukamel, S.; Scopigno, T. Genuine Dynamics vs Cross Phase Modulation Artifacts in Femtosecond Stimulated Raman Spectroscopy. *ACS Photonics* **2019**, *6*, 492−500.
(52) Kang, D.-G.; Woo, K. C.; Kang, D. H.; Park, C.; Kim, S. K. Improved Spectral Resolution of the Femtosecond Stimulated Raman Spectroscopy Achieved by the Use of the 2nd-Order Diffraction Method. *Sci. Rep.* **2021**, *11* (1), 3361.
(53) Frontiera, R. R.; Shim, S.; Mathies, R. A. Origin of Negative and Dispersive Features in Anti-Stokes and Resonance Femtosecond Stimulated Raman Spectroscopy. *J. Chem. Phys.* **2008**, *129*, 64507.
(54) Tang, L.; Liu, W.; Wang, Y.; Zhu, L.; Han, F.; Fang, C. Ultrafast Structural Evolution and Chromophore Inhomogeneity inside a Green-Fluorescent-Protein-Based Ca 2+ Biosensor. *J. Phys. Chem. Lett.* **2016**, *7*, 1225−1230.
(55) Kloz, M.; Van Grondelle, R.; Kennis, J. T. M. Wavelength-Modulated Femtosecond Stimulated Raman Spectroscopy- Approach towards Automatic Data Processing. *Phys. Chem. Chem. Phys.* **2011**, *13*, 18123−18133.

https://doi.org/10.1021/acsphyschemau.3c00031
ACS Phys. Chem Au 2024, 4, 1−18

(56) Grumstrup, E. M.; Chen, Z.; Vary, R. P.; Moran, A. M.; Schanze, K. S.; Papanikolas, J. M. Frequency Modulated Femtosecond Stimulated Raman Spectroscopy of Ultrafast Energy Transfer in a Donor-Acceptor Copolymer. *J. Phys. Chem. B* **2013**, *117*, 8245−8255.
(57) Quincy, T. J.; Barclay, M. S.; Caricato, M.; Elles, C. G. Probing Dynamics in Higher-Lying Electronic States with Resonance-Enhanced Femtosecond Stimulated Raman Spectroscopy. *J. Phys. Chem. A* **2018**, *122*, 8308.
(58) Laimgruber, S.; Schachenmayr, H.; Schmidt, B.; Zinth, W.; Gilch, P. A Femtosecond Stimulated Raman Spectrograph for the near Ultraviolet. *Appl. Phys. B: Laser Opt.* **2006**, *85* (4), 557−564.
(59) Rhinehart, J. M.; Challa, J. R.; McCamant, D. W. Multimode Charge-Transfer Dynamics of 4-(Dimethylamino)Benzonitrile Probed with Ultraviolet Femtosecond Stimulated Raman Spectroscopy. *J. Phys. Chem. B* **2012**, *116* (35), 10522−10534.
(60) Laimgruber, S.; Schmierer, T.; Gilch, P.; Kiewisch, K.; Neugebauer, J. The Ketene Intermediate in the Photochemistry of Ortho-Nitrobenzaldehyde. *Phys. Chem. Chem. Phys.* **2008**, *10* (26), 3872−3882.
(61) Kuramochi, H.; Tahara, T. Tracking Ultrafast Structural Dynamics by Time-Domain Raman Spectroscopy. *J. Am. Chem. Soc.* **2021**, *143* (26), 9699−9717.
(62) Dang, N. C.; Bolme, C. A.; Moore, D. S.; McGrane, S. D. Temperature Measurements in Condensed Phases Using Non-Resonant Femtosecond Stimulated Raman Scattering. *J. Raman Spectrosc.* **2013**, *44* (3), 433−439.
(63) Würthwein, T.; Lüpken, N. M.; Irwin, N.; Fallnich, C. Mitigating Cross-Phase Modulation Artifacts in Femtosecond Stimulated Raman Scattering. *J. Raman Spectrosc.* **2020**, *51* (11), 2265−2271.
(64) Dobner, S.; Cleff, C.; Fallnich, C.; Groß, P. Interferometric Background Reduction for Femtosecond Stimulated Raman Scattering Loss Spectroscopy. *J. Chem. Phys.* **2012**, *137* (17), 174201.
(65) Bradler, M.; Baum, P.; Riedle, E. Femtosecond Continuum Generation in Bulk Laser Host Materials with Sub-μJ Pump Pulses. *Appl. Phys. B: Laser Opt.* **2009**, *97* (3), 561−574.
(66) Dobner, S.; Groß, P.; Fallnich, C. In-Line Interferometric Femtosecond Stimulated Raman Scattering Spectroscopy. *J. Chem. Phys.* **2013**, *138* (24), 244201.
(67) Zhang, W.; Xu, W.; Zhang, G.; Kong, J.; Niu, X.; Chan, J. M. W.; Liu, W.; Xia, A. Direct Tracking Excited-State Intramolecular Charge Redistribution of Acceptor-Donor-Acceptor Molecule by Means of Femtosecond Stimulated Raman Spectroscopy. *J. Phys. Chem. B* **2021**, *125* (17), 4456−4464.
(68) Yoshizawa, M.; Kurosawa, M. Femtosecond Time-Resolved Raman Spectroscopy Using Stimulated Raman Scattering. *Phys. Rev. A* **1999**, *61* (1), 013808.
(69) Jin, S.; Lee, Y. J.; Yu, J. W.; Kim, S. K. Development of Femtosecond Stimulated Raman Spectroscopy: Stimulated Raman Gain via Elimination of Cross Phase Modulation. *Bull. Korean Chem. Soc.* **2004**, *25* (12), 1829−1832.
(70) Krueger, T. D.; Tang, L.; Fang, C. Delineating Ultrafast Structural Dynamics of a Green-Red Fluorescent Protein for Calcium Sensing. *Biosensors* **2023**, *13* (2), 218.
(71) Molesky, B. P.; Guo, Z.; Moran, A. M. Femtosecond Stimulated Raman Spectroscopy by Six-Wave Mixing. *J. Chem. Phys.* **2015**, *142*, 212405.
(72) Beier, H. T.; Noojin, G. D.; Rockwell, B. A. Stimulated Raman Scattering Using a Single Femtosecond Oscillator with Flexibility for Imaging and Spectral Applications. *Opt. Express* **2011**, *19* (20), 18885−18892.
(73) Chung, H.-Y.; Liu, W.; Cao, Q.; Kärtner, F. X.; Chang, G. Er-Fiber Laser Enabled, Energy Scalable Femtosecond Source Tunable from 1.3 to 1.7 μm. *Opt. Express* **2017**, *25* (14), 15760−15771.
(74) Bachler, B. R.; Fermann, M. E.; Ogilvie, J. P. Multiplex Raman Induced Kerr Effect Microscopy. *Opt. Express* **2012**, *20* (2), 835−844.
(75) Kovalenko, S. A.; Dobryakov, A. L.; Ernsting, N. P. An Efficient Setup for Femtosecond Stimulated Raman Spectroscopy. *Rev. Sci. Instrum.* **2011**, *82*, 63102.
(76) Dobryakov, A. L.; Ioffe, I.; Granovsky, A. A.; Ernsting, N. P.; Kovalenko, S. A. Femtosecond Raman Spectra of Cis-Stilbene and Trans-Stilbene with Isotopomers in Solution. *J. Chem. Phys.* **2012**, *137* (24), 244505.
(77) Quick, M.; Dobryakov, A. L.; Kovalenko, S. A.; Ernsting, N. P. Resonance Femtosecond-Stimulated Raman Spectroscopy without Actinic Excitation Showing Low-Frequency Vibrational Activity in the S_2 State of All-Trans β-Carotene. *J. Phys. Chem. Lett.* **2015**, *6* (7), 1216−1220.
(78) Zhu, L.; Liu, W.; Wang, Y.; Fang, C. Sum-Frequency-Generation-Based Laser Sidebands for Tunable Femtosecond Raman Spectroscopy in the Ultraviolet. *Appl. Sci.* **2015**, *5*, 48−61.
(79) Fang, C.; Tang, L.; Oscar, B. G.; Chen, C. Capturing Structural Snapshots during Photochemical Reactions with Ultrafast Raman Spectroscopy: From Materials Transformation to Biosensor Responses. *J. Phys. Chem. Lett.* **2018**, *9* (12), 3253−3263.
(80) Han, F.; Liu, W.; Zhu, L.; Wang, Y.; Fang, C. Initial Hydrogen-Bonding Dynamics of Photoexcited Coumarin in Solution with Femtosecond Stimulated Raman Spectroscopy. *J. Mater. Chem. C* **2016**, *4* (14), 2954−2963.
(81) Weigel, A.; Ernsting, N. P. Excited Stilbene: Intramolecular Vibrational Redistribution and Solvation Studied by Femtosecond Stimulated Raman Spectroscopy. *J. Phys. Chem. B* **2010**, *114* (23), 7879−7893.
(82) McAnally, M. O.; Phelan, B. T.; Young, R. M.; Wasielewski, M. R.; Schatz, G. C.; Van Duyne, R. P. Quantitative Determination of the Differential Raman Scattering Cross Sections of Glucose by Femtosecond Stimulated Raman Scattering. *Anal. Chem.* **2017**, *89* (13), 6931−6935.
(83) Bera, K.; Kwang, S. Y.; Cassabaum, A. A.; Rich, C. C.; Frontiera, R. R. Facile Background Discrimination in Femtosecond Stimulated Raman Spectroscopy Using a Dual-Frequency Raman Pump Technique. *J. Phys. Chem. A* **2019**, *123* (37), 7932−7939.
(84) Rumpel, M.; Moeller, M.; Moormann, C.; Graf, T.; Ahmed, M. A. Broadband Pulse Compression Gratings with Measured 99.7% Diffraction Efficiency. *Opt. Lett.* **2014**, *39* (2), 323−326.
(85) Courtney, T. L.; Mecker, N. T.; Patterson, B. D.; Linne, M.; Kliewer, C. J. Generation of Narrowband Pulses from Chirped Broadband Pulse Frequency Mixing. *Opt. Lett.* **2019**, *44* (4), 835−838.
(86) Dombi, P.; Yakovlev, V. S.; O'Keeffe, K.; Fuji, T.; Lezius, M.; Tempea, G. Pulse Compression with Time-Domain Optimized Chirped Mirrors. *Opt. Express* **2005**, *13* (26), 10888−10894.
(87) Hoffman, D. P.; Valley, D.; Ellis, S. R.; Creelman, M.; Mathies, R. A. Optimally Shaped Narrowband Picosecond Pulses for Femtosecond Stimulated Raman Spectroscopy. *Opt. Express* **2013**, *21* (18), 21685.
(88) Lagutchev, A.; Hambir, S. A.; Dlott, D. D. Nonresonant Background Suppression in Broadband Vibrational Sum-Frequency Generation Spectroscopy. *J. Phys. Chem. C* **2007**, *111* (37), 13645−13647.
(89) Pontecorvo, E.; Ferrante, C.; Elles, C. G.; Scopigno, T. Spectrally Tailored Narrowband Pulses for Femtosecond Stimulated Raman Spectroscopy in the Range 330−750 nm. *Opt. Express* **2013**, *21* (6), 6866−6872.
(90) Shim, S.; Mathies, R. A. Generation of Narrow-Bandwidth Picosecond Visible Pulses from Broadband Femtosecond Pulses for Femtosecond Stimulated Raman. *Appl. Phys. Lett.* **2006**, *89*, 121124.
(91) Co, D. T.; Lockard, J. V.; McCamant, D. W.; Wasielewski, M. R. Narrow-Bandwidth Tunable Picosecond Pulses in the Visible Produced by Noncollinear Optical Parametric Amplification with a Chirped Blue Pump. *Appl. Opt.* **2010**, *49* (10), 1880.
(92) Nejbauer, M.; Radzewicz, C. Efficient Spectral Shift and Compression of Femtosecond Pulses by Parametric Amplification of Chirped Light. *Opt. Express* **2012**, *20* (3), 2136−2142.
(93) Marangoni, M.; Brida, D.; Quintavalle, M.; Cirmi, G.; Pigozzo, F. M.; Manzoni, C.; Baronio, F.; Capobianco, A. D.; Cerullo, G. Narrow-Bandwidth Picosecond Pulses by Spectral Compression of

Femtosecond Pulses in a Second-Order Nonlinear Crystal. *Opt. Express* **2007**, *15* (14), 8884−8891.
(94) Luo, H.; Qian, L.; Yuan, P.; Zhu, H. Generation of Tunable Narrowband Pulses Initiating from a Femtosecond Optical Parametric Amplifier. *Opt. Express* **2006**, *14* (22), 10631−10635.
(95) Lee, J.; Challa, J. R.; Mccamant, D. W. Pump Power Dependence in Resonance Femtosecond Stimulated Raman Spectroscopy. *J. Raman Spectrosc.* **2013**, *44*, 1263.
(96) Liu, W.; Wang, Y.; Tang, L.; Oscar, B. G.; Zhu, L.; Fang, C. Panoramic Portrait of Primary Molecular Events Preceding Excited State Proton Transfer in Water. *Chem. Sci.* **2016**, *7*, 5484−5494.
(97) McCamant, D. W.; Kukura, P.; Mathies, R. A. Femtosecond Time-Resolved Stimulated Raman Spectroscopy: Application to the Ultrafast Internal Conversion in β-Carotene. *J. Phys. Chem. A* **2003**, *107* (40), 8208−8214.
(98) Emons, M.; Steinmann, A.; Binhammer, T.; Palmer, G.; Schultze, M.; Morgner, U. Sub-10-Fs Pulses from a MHz-NOPA with Pulse Energies of 0.4 μJ. *Opt. Express* **2010**, *18* (2), 1191−1196.
(99) Kobayashi, T. Ultrafast Spectroscopy of Coherent Phonon in Carbon Nanotubes Using Sub-5-fs Visible Pulses. *AIP Conf. Proc.* **2016**, *1709* (1), 020001.
(100) Stepanenko, Y.; Radzewicz, C. Multipass Non-Collinear Optical Parametric Amplifier for Femtosecond Pulses. *Opt. Express* **2006**, *14* (2), 779−785.
(101) Laimgruber, S.; Schachenmayr, H.; Schmidt, B.; Zinth, W.; Gilch, P. A Femtosecond Stimulated Raman Spectrograph for the near Ultraviolet. *Appl. Phys. B: Laser Opt.* **2006**, *85*, 557−564.
(102) Tang, L.; Wang, Y.; Zhu, L.; Kallio, K.; Remington, S. J.; Fang, C. Photoinduced Proton Transfer inside an Engineered Green Fluorescent Protein: A Stepwise-Concerted-Hybrid Reaction. *Phys. Chem. Chem. Phys.* **2018**, *20* (18), 12517−12526.
(103) Park, M.; Neukirch, A. J.; Reyes-Lillo, S. E.; Lai, M.; Ellis, S. R.; Dietze, D.; Neaton, J. B.; Yang, P.; Tretiak, S.; Mathies, R. A. Excited-State Vibrational Dynamics toward the Polaron in Methylammonium Lead Iodide Perovskite. *Nat. Commun.* **2018**, *9* (1), 2525.
(104) Roy, P.; Anandan, G. T.; Nayak, N.; Kumar, A.; Dasgupta, J. Raman Snapshots of Side-Chain Dependent Polaron Dynamics in PolyThiophene Films. *J. Phys. Chem. B* **2023**, *127*, 567.
(105) Marx, B.; Czerwinski, L.; Light, R.; Somekh, M.; Gilch, P. Multichannel Detectors for Femtosecond Stimulated Raman Microscopy - Ideal and Real Ones. *J. Raman Spectrosc.* **2014**, *45* (7), 521−527.
(106) Challa, J. R.; Du, Y.; McCamant, D. W. Femtosecond Stimulated Raman Spectroscopy Using a Scanning Multichannel Technique. *Appl. Spectrosc.* **2012**, *66* (2), 227−232.
(107) Knoll, P.; Singer, R.; Kiefer, W. Improving Spectroscopic Techniques by a Scanning Multichannel Method. *Appl. Spectrosc.* **1990**, *44* (5), 776−782.
(108) Frontiera, R. R. *FSRS*. GitHub, 2023. https://github.com/rrflab/FSRS (accessed 2023-07-10).
(109) Dobner, S.; Fallnich, C. Dispersive Fourier Transformation Femtosecond Stimulated Raman Scattering. *Appl. Phys. B: Laser Opt.* **2016**, *122* (11), 278.
(110) Godin, T.; Sader, L.; Khodadad Kashi, A.; Hanzard, P.-H.; Hideur, A.; Moss, D. J.; Morandotti, R.; Genty, G.; Dudley, J. M.; Pasquazi, A.; Kues, M.; Wetzel, B. Recent Advances on Time-Stretch Dispersive Fourier Transform and Its Applications. *Adv. Phys. X* **2022**, *7* (1), 2067487.
(111) Dunbar, J. A.; Osborne, D. G.; Anna, J. M.; Kubarych, K. J. Accelerated 2D-IR Using Compressed Sensing. *J. Phys. Chem. Lett.* **2013**, *4* (15), 2489−2492.
(112) Adhikari, S.; Cortes, C. L.; Wen, X.; Panuganti, S.; Gosztola, D. J.; Schaller, R. D.; Wiederrecht, G. P.; Gray, S. K. Accelerating Ultrafast Spectroscopy with Compressive Sensing. *Phys. Rev. Appl.* **2021**, *15* (2), 024032.
(113) Prince, R. C.; Frontiera, R. R.; Potma, E. O. Stimulated Raman Scattering: From Bulk to Nano. *Chem. Rev.* **2017**, *117* (7), 5070−5094.
(114) Tian, Y.-J.; Zuo, J.; Zhang, L.-Y.; Li, Z.-W.; Gao, S.-Q.; Lu, G.-H. Study of Resonance Raman Cross Section of Aqueous β-Carotene at Low Concentrations. *Appl. Phys. B: Laser Opt.* **2007**, *87* (4), 727−730.
(115) Schomacker, K. T.; Delaney, J. K.; Champion, P. M. Measurements of the Absolute Raman Cross Sections of Benzene. *J. Chem. Phys.* **1986**, *85*, 4240−4247.
(116) Meyer, S. A.; Ru, E. C. L.; Etchegoin, P. G. Quantifying Resonant Raman Cross Sections with SERS. *J. Phys. Chem. A* **2010**, *114* (17), 5515−5519.
(117) Abe, N.; Wakayama, M.; Ito, M. Absolute Raman Intensities of Liquids. *J. Raman Spectrosc.* **1977**, *6* (1), 38−41.
(118) Le Ru, E. C.; Schroeter, L. C.; Etchegoin, P. G. Direct Measurement of Resonance Raman Spectra and Cross Sections by a Polarization Difference Technique. *Anal. Chem.* **2012**, *84* (11), 5074−5079.
(119) Shim, S.; Stuart, C. M.; Mathies, R. A. Resonance Raman Cross-Sections and Vibronic Analysis of Rhodamine 6G from Broadband Stimulated Raman Spectroscopy. *ChemPhysChem* **2008**, *9* (5), 697−699.
(120) Silva, W. R.; Keller, E. L.; Frontiera, R. R. Determination of Resonance Raman Cross-Sections for Use in Biological SERS Sensing with Femtosecond Stimulated Raman Spectroscopy. *Anal. Chem.* **2014**, *86* (15), 7782−7787.
(121) Warkentin, C. L.; Yu, Z.; Sarkar, A.; Frontiera, R. R. Decoding Chemical and Physical Processes Driving Plasmonic Photocatalysis Using Surface-Enhanced Raman Spectroscopies. *Acc. Chem. Res.* **2021**, *54* (10), 2457−2466.
(122) Dumcenco, D.; Huang, Y.-S. The Vibrational Properties Study of Kesterite Cu_2ZnSnS_4 Single Crystals by Using Polarization Dependent Raman Spectroscopy. *Opt. Mater.* **2013**, *35* (3), 419−425.
(123) Singh Bhardwaj, B.; Sugiyama, T.; Namba, N.; Umakoshi, T.; Uemura, T.; Sekitani, T.; Verma, P. Orientation Analysis of Pentacene Molecules in Organic Field-Effect Transistor Devices Using Polarization-Dependent Raman Spectroscopy. *Sci. Rep.* **2019**, *9*, 15149.
(124) Basova, T. V.; Kolesov, B. A. Raman Polarization Studies of the Orientation of Molecular Thin Films. *Thin Solid Films* **1998**, *325* (1−2), 140−144.
(125) Rich, C. C.; Frontiera, R. R. Vibronic Coupling and Exciton Chirality: Electronic and Structural Rearrangement between Helical to Zero Momentum Molecular Exciton States. *J. Phys. Chem. C* **2021**, *125* (39), 21511−21520.
(126) Henry, E. R.; Hofrichter, J. Singular Value Decomposition: Application to Analysis of Experimental Data. In *Methods in Enzymology*; Numerical Computer Methods, Vol. *210*; Academic Press, 1992; pp 129−192.
(127) Kuramochi, H.; Takeuchi, S.; Tahara, T. Ultrafast Structural Evolution of Photoactive Yellow Protein Chromophore Revealed by Ultraviolet Resonance Femtosecond Stimulated Raman Spectroscopy. *J. Phys. Chem. Lett.* **2012**, *3* (15), 2025−2029.
(128) Qi, Y.; Hu, D.; Jiang, Y.; Wu, Z.; Zheng, M.; Chen, E. X.; Liang, Y.; Sadi, M. A.; Zhang, K.; Chen, Y. P. Recent Progresses in Machine Learning Assisted Raman Spectroscopy. *Adv. Opt. Mater.* **2023**, *11* (14), 2203104.
(129) Machado, L. R. P.; Silva, M. O. S.; Campos, J. L. E.; Silva, D. L.; Cançado, L. G.; Vilela Neto, O. P. Deep-Learning-Based Denoising Approach to Enhance Raman Spectroscopy in Mass-Produced Graphene. *J. Raman Spectrosc.* **2022**, *53* (5), 863−871.
(130) Buchanan, L. E.; Gruenke, N. L.; Mcanally, M. O.; Negru, B.; Mayhew, H. E.; Apkarian, V. A.; Schatz, G. C.; Van Duyne, R. P. Surface-Enhanced Femtosecond Stimulated Raman Spectroscopy at 1 MHz Repetition Rates. *J. Phys. Chem. Lett.* **2016**, *7*, 4629−4634.
(131) Buchanan, L. E.; McAnally, M. O.; Gruenke, N. L.; Schatz, G. C.; Van Duyne, R. P. Studying Stimulated Raman Activity in Surface-Enhanced Femtosecond Stimulated Raman Spectroscopy by Varying the Excitation Wavelength. *J. Phys. Chem. Lett.* **2017**, *8* (14), 3328−3333.

(132) Weiner, A. M.; Leaird, D. E.; Wiederrecht, G. P.; Nelson, K. A. Femtosecond Pulse Sequences Used for Optical Manipulation of Molecular Motion. *Science* **1990**, *247* (4948), 1317−1319.
(133) Horstmann, J. G.; Böckmann, H.; Wit, B.; Kurtz, F.; Storeck, G.; Ropers, C. Coherent Control of a Surface Structural Phase Transition. *Nature* **2020**, *583* (7815), 232−236.
(134) Hase, M.; Fons, P.; Mitrofanov, K.; Kolobov, A. V.; Tominaga, J. Femtosecond Structural Transformation of Phase-Change Materials Far from Equilibrium Monitored by Coherent Phonons. *Nat. Commun.* **2015**, *6* (1), 8367.
(135) Endo, M.; Kimura, S.; Tani, S.; Kobayashi, Y. Coherent Control of Acoustic Phonons in a Silica Fiber Using a Multi-GHz Optical Frequency Comb. *Commun. Phys.* **2021**, *4* (1), 73.
(136) Levin, L.; Skomorowski, W.; Rybak, L.; Kosloff, R.; Koch, C. P.; Amitay, Z. Coherent Control of Bond Making. *Phys. Rev. Lett.* **2015**, *114* (23), 233003.
(137) Xia, Y.; Zhao, H.; Zheng, C.; Zhang, S.; Feng, D.; Sun, Z.; Jia, T. Selective Excitation on Tip-Enhanced Raman Spectroscopy by Pulse Shaping Femtosecond Laser. *Plasmonics* **2019**, *14* (2), 523−531.
(138) Shivkumar, S.; Ranann, D.; Metais, S.; Suresh, S.; Forget, N.; Bartels, R.; Oron, D.; Rigneault, H. Selective Detection in Impulsive Low-Frequency Raman Imaging Using Shaped Probe Pulses. *Phys. Rev. Appl.* **2023**, *19* (5), 054075.
(139) Dorfman, K. E.; Schlawin, F.; Mukamel, S. Stimulated Raman Spectroscopy with Entangled Light: Enhanced Resolution and Pathway Selection. *J. Phys. Chem. Lett.* **2014**, *5*, 2843−2849.
(140) Svidzinsky, A.; Agarwal, G.; Classen, A.; Sokolov, A. V.; Zheltikov, A.; Suhail Zubairy, M.; Scully, M. O. Enhancing Stimulated Raman Excitation and Two-Photon Absorption Using Entangled States of Light. *Phys. Rev. Res.* **2021**, *3*, 43029.
(141) Zhang, Z.; Peng, T.; Nie, X.; Agarwal, G. S.; Scully, M. O. Entangled Photons Enabled Time-Frequency-Resolved Coherent Raman Spectroscopy and Applications to Electronic Coherences at Femtosecond Scale. *Light Sci. Appl.* **2022**, *11* (274), 2047−7538.
(142) Pu, R.; Wang, Z.; Zhu, R.; Jiang, J.; Weng, T.-C.; Huang, Y.; Liu, W. Investigation of Ultrafast Configurational Photoisomerization of Bilirubin Using Femtosecond Stimulated Raman Spectroscopy. *J. Phys. Chem. Lett.* **2023**, *14* (3), 809−816.

https://doi.org/10.1021/acsphyschemau.3c00031
ACS Phys. Chem Au 2024, 4, 1−18